Anatomy and phylogenetic relationships of a possible lessemsaurid with associated plant fossils from the lower part of the Elliot Formation

Atashni Moopen[1*] §, Aviwe Matiwane[2], Pia A. Viglietti[1,3] & Jonah N. Choiniere[1]

[1]*Evolutionary Studies Institute, and School of Geosciences, University of the Witwatersrand, Private Bag 3, WITS, Johannesburg, 2050 South Africa*

[2]*Extended Studies Unit, Centre of Higher Education Teaching and Learning, Rhodes University, P.O. Box 94, Makhanda, Eastern Cape, 6140 South Africa, and Earth Sciences Department, Albany Museum, 40 Somerset St, Makhanda, 6139 South Africa*

[3]*Negaunee Integrative Research Center, Field Museum of Natural History, 1400 South Lake Shore Drive, Chicago, IL, 60605, United States*

Received 6 July 2023. Accepted 27 November 2023

The Elliot Formation forms the middle layer of the Stormberg Group of South Africa and ranges in age from the Upper Triassic to the Lower Jurassic. This stratigraphic unit bears a rich and varied faunal assemblage, including a wide variety of vertebrate fossils, the most abundant of which are sauropodomorph dinosaurs. While Early Jurassic sauropodomorphs are increasingly well-known, our knowledge of Late Triassic sauropodomorphs from the lower Elliot Formation is still at a deficit. Specimens from this section of the Stormberg Group can provide key information on the early evolution of Sauropodomorpha. Here we report on a new specimen of a Late Triassic sauropodomorph from a locality a short distance above the Molteno–Elliot boundary making it among the stratigraphically lowest sauropodomorphs from South Africa. Phylogenetic analyses and body mass estimations indicate the specimen represents a medium-to-large-bodied possible lessemsaurid with a combination of plesiomorphic and derived characters. This specimen adds to the diversity of the lower Elliot Formation and provides stronger support for a biogeographical link between the Elliot Formation and the Los Colorados Formation of Argentina. This skeletally immature possible lessemsaurid also provides insight into body size evolution during the Norian, a critical time for the evolution of sauropodomorph gigantism. The fossil plant genera *Taeniopteris* and *Cladophlebis* were recovered from sediments containing the sauropodomorph specimen, documenting one of the first co-occurrences of dinosaurs and plant material in the Elliot Formation, as well as preserving direct evidence of plant–insect interactions.

Keywords: Sauropodomorpha, Late Triassic, lower Elliot Formation, Norian, Lessemsauridae, *Taeniopteris*, *Cladophlebis*.

INTRODUCTION

The Elliot Formation (EF) overlies the Molteno and underlies the Clarens formations as the middle unit of the Stormberg Group within the upper Karoo Supergroup (Bordy & Eriksson 2015; Kitching & Raath 1984). The EF is informally subdivided into lower (lEF) and upper (uEF) sections based on lithostratigraphic distinctions (summarized in Bordy & Eriksson 2015) that generally correspond with biostratigraphic changes (Kitching & Raath 1984; Viglietti *et al*. 2020a,b). The EF represents a temporal range from the Late Triassic (Norian–Rhaetian) to Early Jurassic (Hettangian–Sinemurian), which encompasses the end-Triassic extinction (Olsen & Galton 1984; Bordy *et al*. 2020).

The EF contains a diverse faunal assemblage across a range of taxa (e.g. Haughton 1924; Kitching & Raath 1984; Viglietti *et al*. 2020a,b), and is biostratigraphically divided into the *Scalenodontoides* and *Massospondylus* Assemblage Zones, which mostly correspond with the lEF/uEF, respectively. The most common vertebrate fossils across the EF are members of the clade Sauropodomorpha, saurischian dinosaurs that are well known for their large body sizes (Benson *et al*. 2014). Recent research on EF sauropodomorphs has resulted in breakthroughs on sauropodomorph posture (McPhee *et al*. 2018, Chapelle *et al*. 2020); body mass evolution (Benson *et al*. 2014; Benson *et al*. 2017; Apaldetti *et al*. 2018; McPhee *et al*. 2018); growth strategies (Cerda *et al*. 2017; Chapelle *et al*. 2021; Botha *et al*. 2022); and taxonomy (e.g. Apaldetti *et al*. 2018; Barrett *et al*. 2019; Chapelle *et al*. 2019; Griffin *et al*. 2022). This group of dinosaurs is potentially among the most useful global dinosaurian biostratigraphic markers in the Late Triassic (McPhee *et al*. 2017), but the current taxonomic and phylogenetic data for sauropodomorphs of this period are in a state of flux (McPhee *et al*. 2015a, 2017).

Non-sauropodan sauropodomorphs are also interesting from a functional anatomy perspective and they display a

*Author for correspondence. E-mail: tashmoopen@gmail.com

wide range of body sizes and postures from bipedal to quadrupedal (McPhee *et al*. 2018). Most early branching sauropodomorphs have been identified as small-bodied and shifted to larger-bodied taxa within the Triassic, and this shift is observed more frequently within Sauropodomorpha than in other dinosaurian clades (Benson *et al*. 2017; Apaldetti *et al*. 2018; Apaldetti *et al*. 2021). The earliest South African sauropodomorph specimens could provide insight into the pattern of diversification, biogeographic relationships, and the early evolutionary history of Sauropodomorpha (Pol & Powell 2007).

Recent research into South African sauropodomorph diversity includes the discovery of new genera (McPhee *et al*. 2018; Chapelle *et al*. 2019; Peyre de Fabrègues & Allain 2020) that contributed to the information on the Early Jurassic section of the EF, but the same has not been done for the Late Triassic. In contrast, the fossil record of the Late Triassic Formations in Argentina, e.g. the Ischigualasto and Los Colorados formations, are richer and well researched, yielding an excellent fossil record of early branching sauropodomorphs (Bonaparte 1971; Apaldetti *et al*. 2018; Pol *et al*. 2021b; Otero & Hutchinson 2022). The difference in the quality of the fossil record between these formations makes them challenging to compare, as they have little to no overlap in genus or species-level taxa. Sauropodomorphs from the Norian–Rhaetian of South Africa have the potential to provide better biostratigraphic links to deposits in Argentina, given their closer temporal correspondence (Pol & Powell 2007).

Lessemsauridae is a Gondwanan clade of non-sauropodan sauropodomorphs from South Africa, Lesotho, and Argentina. This clade is variably considered to be the sister taxon of Sauropoda or to branch very close to sauropod origins. Lessemsaurids bear a unique combination of plesiomorphic and derived morphological features, which together with their phylogenetic placement positions them as a key taxon for understanding the evolution of Sauropoda (Pol & Powell 2007; Apaldetti & Martínez 2022). For example, research on lessemsaurids has suggested that they had avian-like respiratory systems, lacked fully erect forelimb postures, and developed large body sizes and quadrupedality independently from Sauropoda (Pol & Powell 2007; Apaldetti *et al*. 2018; McPhee *et al*. 2018; Apaldetti & Martínez 2022).

Body mass is related to the physiological and ecological properties of an animal and can provide inference and palaeobiological reconstructions of extinct taxa (Campione & Evans 2012; Campione *et al*. 2014; Benson *et al*. 2017). The broadest studies of sauropodomorph body mass employ limb bone scaling methods, most recently based on regression models of limb robusticity (Campione & Evans 2012; McPhee *et al*. 2018; Chapelle *et al*. 2020). In these models, the circumference of stylopodial elements is measured and body mass is estimated with reference to regression models based on extant taxa of known body mass. This method can be used with even partial remains (Anderson *et al*. 1985; Campione & Evans 2012; Benson *et al*. 2014, 2017; Campione *et al*. 2014).

Diverse fossil floras are known from the Permian and Middle Triassic of South Africa (e.g. Anderson & Anderson 1985), but plant fossils in the EF are rare, comprising only fossilized wood of large gymnosperms (Bordy *et al*. 2004), rhizoliths (Sciscio *et al*. 2021), and fragmented leaves (Anderson & Anderson 1985). Records of dinosaur–plant co-occurrences or other plant–animal interactions are generally uncommon for earlier Mesozoic ecosystems, and are currently unknown for the EF. Because of these deficits, we have a poor understanding of the vegetative environment in the EF of South Africa.

This study describes the partial skeleton of a sauropodomorph specimen (BP/1/8489) recovered from the lEF approximately 20 metres above the Molteno contact, making it one of the stratigraphically lowest known occurrences of a sauropodomorph body fossil in South Africa. The sediments containing BP/1/8489 contain abundant leaves of the fernlike fossil plant genera *Taeniopteris* and *Cladophlebis*, representing the first known co-occurrence of an EF dinosaur with vegetative material. The skeleton displays a combination of derived and plesiomorphic sauropodomorph features suggesting that it is a Late Triassic (Norian) lessemsaurid, the first occurrence of this taxon in the lEF of South Africa.

GEOLOGICAL SETTING

BP/1/8489 was found *in situ* in Joe Gqabi District, on Teeken Fontein (Cadastral farm number 68) near the village of Rossouw in the Eastern Cape Province, South Africa (Fig. 1B) and was collected in successive field seasons from 2017 to 2018. The specimen was found on the low-water margin of an artificial dam, in a small piece of original outcrop of the lEF (31.166426°S; 27.103161°E). Its remains were disarticulated but densely clustered in a 2 m thick fine greenish grey (5YR 5/2) finely bedded siltstone and in association with locally abundant plant leaf beds comprising six leaf morphospecies. The siltstone was down-cut by a medium-grained sandstone channel that increased in thickness to ~2 m, comprising lateral accretion architectural elements and 1 m thick trough cross-beds. Thus, the depositional environment is interpreted to consist of an avulsing, laterally accreting channel, which later became abandoned and infilled with the siltstone, disarticulated bones, and plant material, potentially under high energy conditions (Fig. 2) of the lower Elliot Formation (lEF) approximately 20 metres above the Molteno–Elliot contact (Fig. 1A).

MATERIAL

BP/1/8489 is an assemblage of associated but disarticulated postcranial material pertaining to a single skeletally immature sauropodomorph individual. The postcranial material is congruent in size and morphology and we hypothesize it represents a single individual. The material includes two dorsal neural arches, four caudal vertebrae, a left scapula, a right postacetabular process of the ilium, a left pubic peduncle, a partial right femur and a left femoral head, two phalanges, and an ungual. Many of the elements are badly broken or missing portions of their cortical bone. The disorganized preservation of the material (i.e. without articulation and with disparate

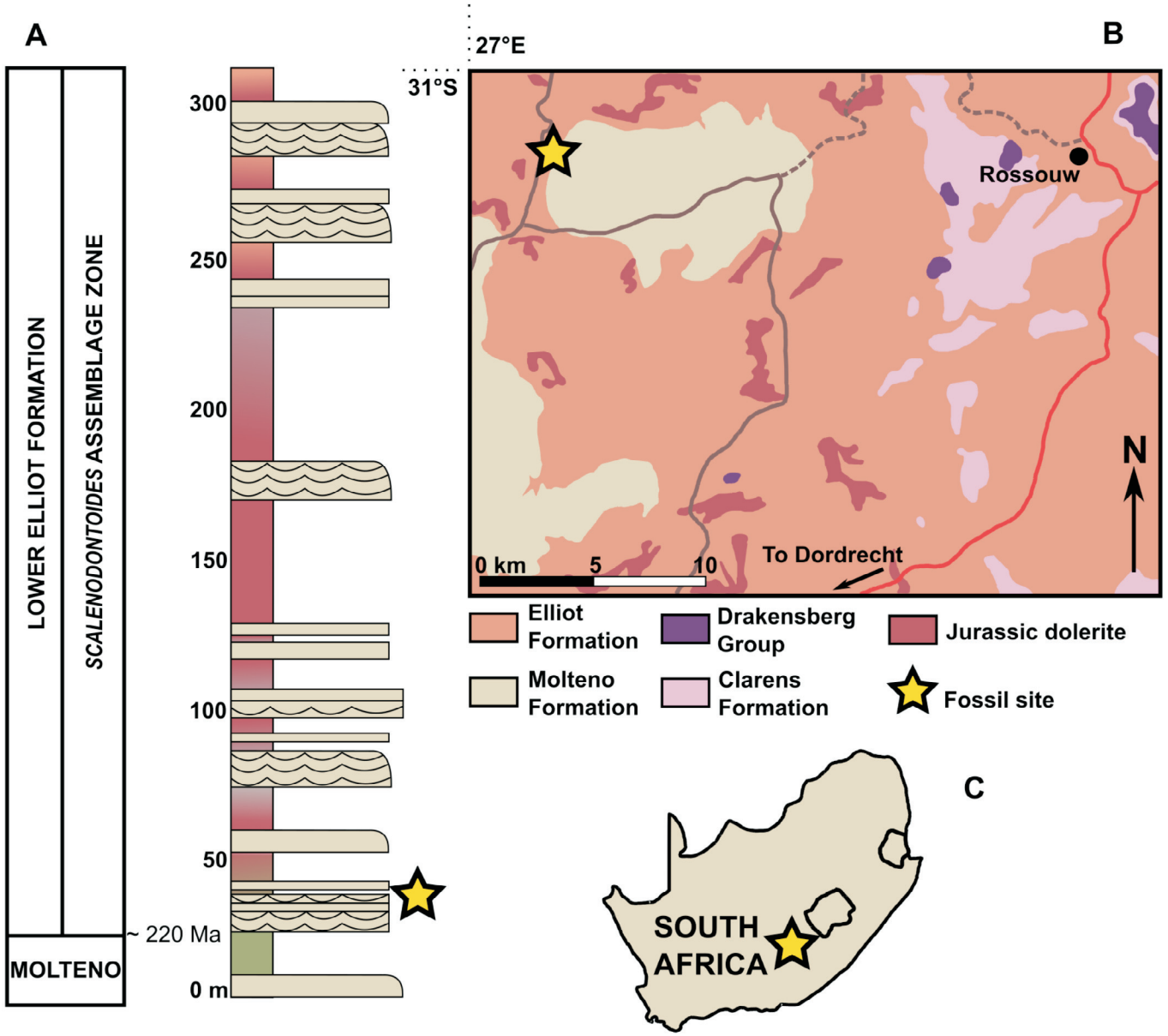

Figure 1. Geological context of BP/1/8489. **A**, The inferred stratigraphic position of BP/1/8489 on Teeken Fontein 68. The vertical section represents a composite section measured at the fossil site on Teeken Fontein 68 (Molteno contact), and Driefontein 41 (lEF; –31.084915S; 27.212528E). **B**, **C**, Locality of BP/1/8489. Light brown = Elliot Formation; Purple = Drakensberg; Dark brown = Jurassic Dolerite; Beige = Molteno Formation; Pink = Clarens Formation; Yellow star = Fossil site.

elements lying on top of one another) and the erosion of some of the bones suggest it was transported a short way before being preserved (Fig. 2).

Plant material preserved with the specimen was saved during the preparation process, and larger blocks of siltstone were split along cleavage planes to search for the highest fidelity of leaf impressions. A total of 18 slabs containing plant material were recovered, some of which contain multiple leaf impressions.

METHODS

Most of the bones of the skeleton were fully contained within matrix and underwent preparation with pneumatic air scribes. Bones exposed from the matrix were consolidated using a solution of 10% (weight/volume) paraloid copolymer B-76 dissolved in acetone.

Descriptions of BP/1/8489 are based on all preserved elements, with vertebral descriptions based on the best-preserved elements of the respective anatomical sections, supplemented with descriptive information from other elements that preserved key portions of the anatomy. Anatomical comparisons (Table 1) were based on literature and observations of specimens of other sauropodomorph taxa from the Karoo Collections of the Evolutionary Studies Institute. The Argentinian lessemsaurid *Ingentia prima* was considered for comparison, but has little overlap in preserved elements with BP/1/8489.

We employ non-standardized Romerian terminology in our descriptions (e.g. anterior/posterior, dorsal/ventral, medial/lateral for major anatomical directions). We generally use the adjectives 'long' and 'short' to refer to variation in the anteroposterior direction, 'tall' and 'low' to refer to variation in the dorsoventral direction, and 'wide' and 'narrow' to refer to variation in the mediolateral direction. When we depart from these conventions, we provide specific directional terms to modify the adjectives. Verte-

Figure 2. **A**, The locality where BP/1/8489 was discovered, on the low water margin of an artificial dam on the farm Teeken Fontein 68, near Rossouw, Eastern Cape Province. The plant and dinosaur bone-bearing fossil site, which lies in finely bedded siltstone, is adjacent to a 2m thick channel sandstone showing lateral accretion architectural elements. **B**, Site map and sedimentological data of the fossil bone and plant material. Note that the fossils were found in green siltstone, and plant fossil beds were often in close association with the bones of BP/1/8489. The site was also located immediately adjacent to the sandstone channel, and interpreted as representing abandoned channel fill. Photo source: Pia Viglietti.

Table 1. List of vertebrate comparative taxa with their source(s).

Taxon	Source(s)
Aardonyx celestae	BP/1/6250, 6510, 6566, 6595, 6641, 6666, 6670
Antetonitrus ingenipes	BP/1/4952
Eucnemesaurus entaxonis	BP/1/6234
Ingentia prima	Apaldetti *et al.* (2018)
Kholumolumo ellenbergerorum	Peyre de Fabrègues & Allain (2020)
Ledumahadi mafube	BP/1/7120
Lessemsaurus sauropoides	Pol & Powell (2007)
Massospondylus carinatus	BP/1/4934
Melanorosaurus readi	Galton *et al*. (2005); NMQR 1551
Meroktenos thabanensis	Peyre de Fabrègues & Allain (2016)
Mussaurus patagonicus	Otero & Pol (2013)
Pulanesaura eocollum	BP/1/6183a, 6186, 6201, 6646, 6982
Riojasaurus incertus	Bonaparte (1971)
Sefapanosaurus zastronensis	BP/1/7409–7455
Yunnanosaurus huangi	Young (1942)

bral laminae and fossae names are based on Wilson's terminology (Wilson 1999; Wilson *et al*. 2011).

Plant fossils were brushed gently to remove adhering soil and sediments, and photographed on a Canon EOS77D equipped with a L-series 24–105 mm lens under a variety of raking light angles. Images of plants were sharpened, colour-corrected, cropped and rotated, but otherwise unaltered and no morphological features were changed or enhanced during image processing. Plant fossil anatomy was compared to the published literature to make identifications.

We conducted phylogenetic analyses using the maximum parsimony criterion to assess the phylogenetic relationships of BP/1/8489. We scored BP/1/8489 in the McPhee *et al*. (2018) character matrix that comprises 61 taxa and 366 discrete morphological characters as well as in the character matrix of Pol *et al*. (2021a) with 77 taxa and 419 discrete morphological characters, some of which were treated as ordered (see Supplement S1). The character matrices were maintained in Mesquite (Maddison & Maddison 2019) and analysed in TNT (Tree Analysis for New Technology; Goloboff & Catalano 2016) using a heuristic search of 1000 replicates of Wagner trees (random seed 1) with TBR (tree bisection reconnection) branch swapping algorithm with two trees saved per replication. An additional round of TBR was conducted on the most parsimonious trees (MPTs) from this search with the 'collapse' option on the search. Additionally, implied weighting analyses (Goloboff *et al*. 2008) were conducted on both character datasets in TNT using concavity functions of $k = 3$ and $k = 6$, and a constrained analysis enforcing the monophyly of Lessemsauridae inclusive of BP/1/8489 within the Pol *et al*. (2021a) dataset. To assess the robustness of the phylogenetic hypothesis for BP/1/8489 we used TNT to calculate Bremer support values (Bremer 1994), saving suboptimal trees up to five steps longer than MPTs for both character datasets. We also calculated Bootstrap support values in TNT using 100 replicates and symmetric resampling. Using MPTs and ages of taxa drawn from McPhee *et al*. (2018) and Pol *et al*. (2021a), the phylogenies was then imported into R Studio to create time-calibrated phylogenies using the *strap* (Bell *et al*. 2022) and *geiger* packages (Harmon *et al*. 2007).

Body mass (BM) estimation analyses were conducted based on the measurements of the relatively complete femur; however, the complete circumference could not be measured. In order to estimate the femoral circumference, we compiled a database of 53 sauropodomorph taxa, using measurements from Benson *et al*. (2014) and personal research, with known mediolateral diameter of the femoral shaft and femoral circumferences (see S2). We made a linear regression model using R Studio (v.4.2.0) to

Table 2. Body mass equations and their source(s).

	Source(s)	Equations
Quadrupedal	Campione & Evans (2012)	$Log_{10}BM = 2.818 \cdot Log_{10}C_f - 0.417$
Bipedal	Campione *et al*. (2014)	$Log_{10}BM = 2.754 \cdot Log_{10}C_f - 0.683$

determine a relationship between the log_{10} of the mediolateral diameter of the femoral shaft and the log_{10} of the femoral circumference, and used this to estimate the femoral circumference of BP/1/8489 (Fig. 9).

Mass estimations were done using equations for both quadrupedal and bipedal postures, as a forelimb was not preserved, posture could not be determined for BP/1/8489. The body mass estimations are based on the scaling equations of Campione & Evans (2012) for extant quadrupedal vertebrates, and Campione *et al*. (2014) for extant bipedal vertebrates using femoral circumference (see Table 2).

Table 3. Measurements of the skeletal elements of BP/1/8489.

Skeletal elements	Measurement taken	mm
Scapula	dorsoventral height	490
	minimum anteroposterior length	102
Dorsal vertebra	total dorsoventral height	216
	neural spine: height from base	130
	neural spine: anteroposterior length	87
Caudal vertebra	total dorsoventral height	340
	dorsoventral height of centrum	140
	width of centrum (posterior)	105
	anteroposterior length of centrum	92
	neural spine: height from base	174
	neural spine: anteroposterior length	56.4
	transverse process length	106
Femur	minimum mediolateral length (diameter)	108
	dorsoventral length	778
Manual phalanx	proximodistal length	51.5
	proximal transverse width	58
	proximal dorsoventral length	46.9
Pedal phalanx	proximodistal length	78.7
	transverse width	53
	dorsoventral length	43

RESULTS

Systematic palaeontology

Dinosauria Owen, 1842
Saurischia Seeley, 1888
Sauropodomorpha Huene, 1932
Lessemsauridae Apaldetti *et al*. 2018

Anatomical description of BP/1/8489

Anterior dorsal neural arch

The neural arch of a dorsal vertebra is well-preserved but is lacking the dorsal half of the neural spine and the right transverse process (Fig. 3). The middle of the neurocentral sutural region is preserved with its anterior end, the posterior end of the postzygapophyses, and an eroded hyposphene. The long neural spine and lack of parapophysis suggests a position among the anterior vertebrae of the dorsal series. The base of the neural spine has been deformed so that it is off centre towards the left making it impossible to determine its direction, lamination, or any basic proportions (see Table 3 for measurements). Weakly developed spinoprezygapophyseal laminae (sprl) are present at the base of the neural spine.

The neural arch has posterior centrodiapophyseal laminae (pcdl) and postzygodiapophyseal laminae (podl) with no accessory lamination. The podl is the dorsoventrally thinnest lamina present. The neural canal of the anterior dorsal neural arch is dorsoventrally taller than it is wide with the lateral walls medially concave. This is similar to the condition in *Massospondylus* (BP/1/4934), *Eucnemesaurus* (McPhee *et al*. 2015b), and *Kholumolumo* (Peyre de Fabrègues & Allain 2020), considered here as a lessemsaurid, whereas in *Antetonitrus* (BP/1/4952) and more derived sauropodomorphs (e.g. *Tazoudazaurus*, Allain & Aquesbi 2008), the neural canal is high and slot-shaped with vertical walls. The pedicle of the dorsal neural arch is not as tall in proportion to that of *Antetonitrus* (BP/1/4952) but is similar to *Massospondylus* (BP/1/4934).

The transverse process is robust but its distal end is abraded, although it is mediolaterally short. The dorsal surface of the transverse process is strongly convex and the ventral surface is supported by a vertically erect pcdl. The anterior centrodiapophyseal lamina (acdl) is robust and extends from the neurocentral suture at an approximate 45° angle to meet the ventral surface of the transverse process. A prezygodiapophyseal lamina (prdl) extends from the lateral margin of the prezygapophysis to the anterior margin of the transverse process, forming a broad triangular area in dorsal view. A prezygocentrodiapophyseal fossa (prcdf) and postzygocentrodiapophyseal fossa (pocdf) are present ventral to the transverse process. Both fossae are deep with the prcdf triangular in anterior view and the pocdf is anteroposteriorly long.

The prezygapophyses extend anterodorsally beyond the level of the anterior margin of the neural arch pedicle. The prezygapophyses extend laterally with what appears to be elliptical prezygapophyseal facets in dorsal view. The prezygapophyses bear a well-developed hypantrum, which based on its distal margin is keyhole shaped in dorsal view. Hyposphene–hypantrum articulations are common in many sauropodomorphs, such as *Massospondylus* (BP/1/4934), *Antetonitrus* (BP/1/4952), *Mussaurus* (Otero & Pol 2013), *Riojasaurus* (Bonaparte 1971), and *Pulanesaura* (BP/1/6183a). The medial surface of the hypantrum walls are subrectangular and form near-vertical faces, similarly to *Aardonyx* (BP/1/6566). The weakly developed sprl converge at the base of the neural spine and between this convergence at the base of the prezygapophyses is a mediolaterally narrow, dorsoventrally tall spinoprezygapophyseal fossa (sprf). The postzygapo-

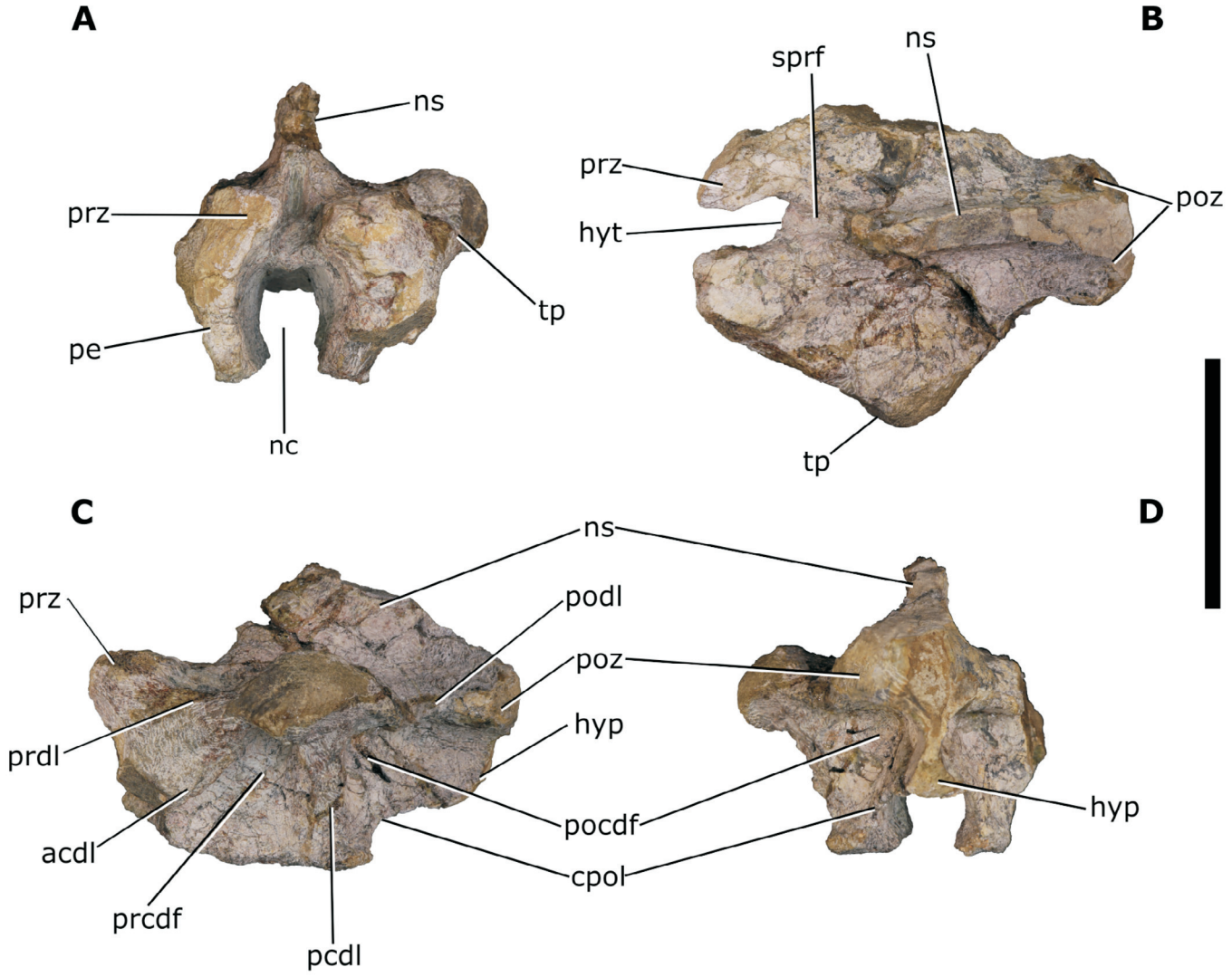

Figure 3. Anterior dorsal neural arch of BP/1/8489. **A**, anterior; **B**, dorsal; **C**, left lateral; and **D**, posterior views. Abbreviations: acdl, anterior centrodiapophyseal lamina; cpol, centropostzygapophyseal lamina; hyp, hyposphene; hyt, hypantrum; nc, neural canal; ns, neural spine; pcdl, posterior centrodiapophyseal lamina; pe, pedicle; pocdf, postzygocentrodiapophyseal fossa; podl, postzygodiapophyseal lamina; poz, postzygapophyses; prcdf, prezygocentrodiapophyseal fossa; prdl, prezygodiapophyseal lamina; prz, prezygapophyses; spol, spinopostzygapophyseal lamina; sprf, spinoprezygapophyseal fossa; sprl, spinoprezygapophyseal lamina; tp, transverse process. Scale bar = 10 cm.

physes extend posteriorly well beyond the posterior margin of the neural arch pedicle and are directed ventrolaterally. The postzygapophyseal facets are aligned with the horizontal axis in posterior view and have smooth elliptical facets in ventral view. A hyposphene is present ventral to the postzygapophyses (Fig. 3D). The hyposphene is well-developed, and triangular in posterior view with its ventral surface as mediolaterally broad as the neural canal, similar to *Antetonitrus* (BP/1/4952), *Massospondylus* (BP/1/4934), and *Aardonyx* (BP/1/6566). A salient feature of the anterior dorsal neural arch is that the centropostzygapophyseal laminae (cpol) are well developed and merge with the ventrolateral margins of the hyposphene as a prominent sheet of bone (Fig. 3C,D), similarly to *Kholumolumo* (Peyre de Fabrègues & Allain 2020).

Posterior dorsal neural arch

The posterior dorsal neural arch of BP/1/8489 is missing the anterodorsal portion of the neural spine, the prezygapophyseal articular facets, the left postzygapophysis, and the distal end of the right transverse process (Fig. 4). The neural spine has a slight distortion to the right (Fig. 3A).

The neural spine is 1.34 times taller than it is long, similar to the ratio seen in *Lessemsaurus* (Pol & Powell 2007) and *Melanorosaurus* (Galton *et al*. 2005), but lower than the ratio of 1.5 seen in *Antetonitrus* (BP/1/4952) and 2.0 in *Ledumahadi* (BP/1/7120). The neural spine widens mediolaterally and lengthens towards its distal end, forming a 'spine table', similar to that of *Antetonitrus* (BP/1/4952). The anterior margin of the neural spine tapers and forms an acute angle. The posterior margin of the neural spine bows posteriorly so that it is concave in lateral view, similar to *Antetonitrus* (BP/1/4952) and *Ledumahadi* (BP/1/7120). The posterodorsal corner of the distal end of the neural spine extends posteriorly to the margin of the postzygapophyses. The base of the neural spine in anterior view does not suggest it was similarly expanded as the posterior side. A teardrop-shaped sprf is present at the base of the neural spine.

The neural canal is subcircular in posterior view, similar

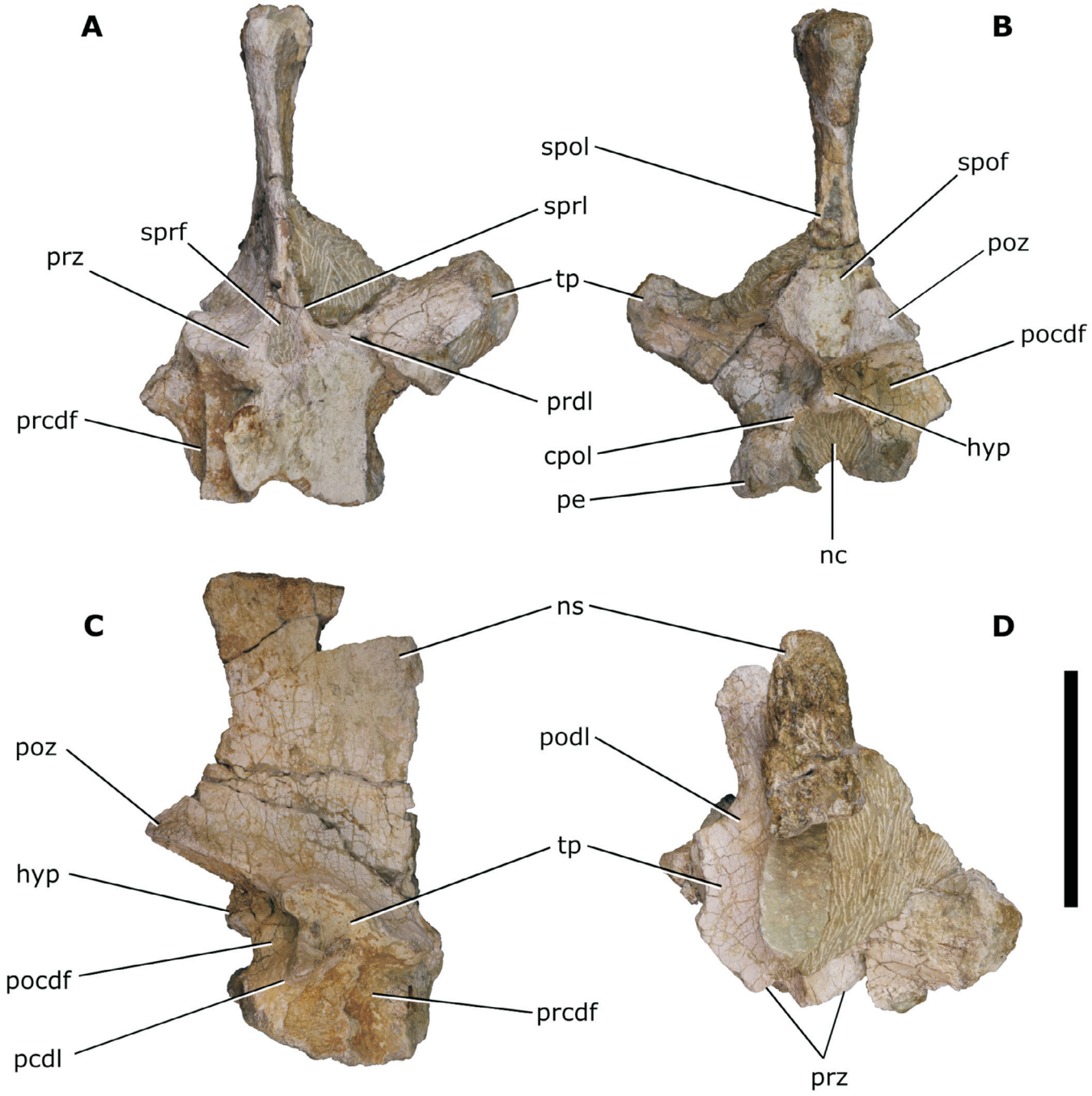

Figure 4. Posterior dorsal neural arch of BP/1/8489. **A**, anterior; **B**, posterior; **C**, right lateral; and **D**, dorsal views. Abbreviations: cpol, centropostzygapophyseal lamina; hyp, hyposphene; nc, neural canal; ns, neural spine; pcdl, posterior centrodiapophyseal lamina; pe, pedicle; pocdf, postzygocentrodiapophyseal fossa; podl, postzygodiapophyseal lamina; poz, postzygapophyses; prcdf, prezygocentrodiapophyseal fossa; prdl, prezygodiapophyseal lamina; prz, prezygapophyses; spof, spinopostzygapophyseal fossa; spol, spinopostzygapophyseal lamina; sprf, spinoprezygapophyseal fossa; sprl, spinoprezygapophyseal lamina; tp, transverse process. Scale bar = 10 cm.

to that of *Eucnemesaurus* (McPhee *et al*. 2015b) and *Massospondylus* (BP/1/4934), but contrasting the slit-shaped neural canal of *Antetonitrus* (BP/1/4952). The cpol along the neural canal is rounded and prominent, extending slightly posteriorly from the rest of the neural arch and continuing onto the base of the hyposphene.

The transverse process extends dorsolaterally and is directed anteriorly. The dorsal surface is convex near its base. The distal end is bulbous, with the dorsal margin weakly convex and the ventral margin strongly convex. The ventral surface is supported by a robust pcdl, although the anterior margin of the transverse process is not preserved, an acdl is likely present.

The prezygapophyses can be inferred to have diverged laterally based on the direction of the sprl that are angled anterolaterally. The sprl are thin sheets that converge at the very base of the neural spine. The postzygapophyses extend posteriorly beyond the posterior margin of the neural spine and well beyond the neural arch pedicle. The postzygapophyseal articular facets are angled at approximately 20° from the horizontal. The postzygapophyseal facets are elliptical and directed ventrolaterally. A salient feature of the facets is that they are autapomorphically long (Fig. 4C), in ventral view they form an anteroposteriorly long ellipse, and their lateral surface is confluent with the broad ventral surface of the podl.

Postzygapophyseal articular facets are usually circular or elliptical like those of *Massospondylus* (BP/1/4934) and *Mussaurus* (Otero & Pol 2013). The spinopostzygapophyseal laminae (spol) are prominent and extend all the way to the midlength of the neural spine. The spol frame a deep, tall, triangular spinopostzygapophyseal fossa (spof) between the postzygapophyses. This is similar to many early branching sauropodomorphs such as *Riojasaurus* (Bonaparte 1971), *Aardonyx* (BP/1/6666), *Mussaurus* (Otero & Pol 2013), and *Antetonitrus* (BP/1/4952), but is not as developed and distinct as in *Pulanesaura* (BP/1/6183a). The hyposphene has a similar triangular morphology as the anterior dorsal neural arch, with the ventral surface narrower than the width of the neural canal. The hyposphene also does not extend as far distally; it is anteroposteriorly shorter than the hyposphene in the anterior dorsal.

Two deep fossae are present: a pocdf that has main subsidiary fossa within it (Fig. 4B), one located more anterior and laterally on the posterior surface of the pcdl and the second subsidiary fossa located on the lateral surface of the hyposphene. A deep, hemispherical prcdf is present ventral to the transverse process (Fig. 4C).

Anterior caudal vertebra

Multiple anterior caudal vertebrae are associated with BP/1/8489 that are similar in morphology. Four caudal vertebrae preserve the neural spine, centrum, and transverse processes. Three more of the caudal vertebrae are fragile and can only be partially prepared from mudstone matrix, these have zygapophyses that are weathered or broken. The best-preserved anterior caudal vertebra (Fig. 5) is relatively complete with small fragments missing along the anterior and posterior margins of the neural spine, with some erosion on the distal ends of the transverse processes and postzygapophyses. The centrum has evidence of weathering and missing fragments along the margins of its articular surfaces of both the anterior and posterior surfaces with some mudstone left on the centre of the anterior articular surface.

The neural spine is tall, mediolaterally thin, and anteroposteriorly short, being 2.8 times taller than it is long. The neural spine slopes posterodorsally (Fig. 5D), similarly to that of *Kholumolumo* (Peyre de Fabrègues & Allain 2020). The anterior and posterior margin of the neural spine tapers, creating a prespinal (prsl) and postspinal (posl) lamina, respectively. This neural lamination is not seen in *Antetonitrus* (BP/1/4952) or *Massospondylus* (BP/1/4934), but is observed in *Kholumolumo* (Peyre de Fabrègues & Allain 2020). The distal end of the neural spine expands mediolaterally. The neural arch is confluent with the anterior surface of the centrum, with the posterior surface slightly beyond the posterior margin of the neural arch. The neural canal is wider than it is tall, almost heart-shaped in anterior view compared to the tall elliptical outline of the neural canal in the dorsal neural arches.

The transverse processes are dorsoventrally flattened, and weakly curve dorsally as they extend posterolaterally so that the dorsal surface is concave and the ventral surface is convex (Fig. 5A,C). This curve in the transverse processes is not common in sauropodomorphs and is possibly a local autapomorphy in later-branching sauropodomorphs such as *Pulanesaura* (BP/1/6201). The transverse processes lack laminae.

The prezygapophyses extend anteriorly beyond the level of the anterior margin of the centrum while the postzygapophyses extend posteriorly slightly beyond the posterior margin. The prezygapophyseal articular facets are partially obscured by matrix but appear elliptical in dorsal view and are angled dorsomedially at approximately 45°. An intraprezygapophyseal lamina (tprl) is present between the prezygapophyses, it is a thin sheet of bone that connects the bases of the prezygapophyses. The postzygapophyses are located on the base of the neural spine rather than the neural arch. The postzygapophyses are angled at approximately 45° from the horizontal and have articular facets that are elliptical in ventral view. A wide and narrow intrapostzygapophyseal lamina (tpol) extends along the distal margins of the postzygapophyses connecting them together, and is continuous with the hyposphene, similarly to that of *Antetonitrus* (BP/1/4952). A mediolaterally broad, shallowly convex hyposphene is confluent with the tpol and connects it to the dorsal margin of the neural canal. The posterior surface of the hyposphene is angled at 45°. The hyposphene in BP/1/8489 is weakly developed in comparison to the prominent hyposphene seen in *Antetonitrus* (BP/1/4952). Weakly developed sprl and spol can be identified on the anterior caudal as well as the other caudal vertebrae. The sprl weakly join on the lateral sides of the neural spine.

The centrum is taller than it is long with a length/height ratio of 0.66, similar to that of *Antetonitrus* (BP/1/4952). The anterior articular surface of the centrum is elliptical and the posterior surface is rectangular in anterior and posterior views, respectively, and these surfaces are both dorsoventrally taller than they are mediolaterally wide. The anterior articular surface is deeply concave, whereas the posterior articular surface is shallowly convex resulting in a weakly procoelous centrum, similar to those of *Ledumahadi* (BP/1/7120) and *Riojasaurus* (Bonaparte 1971). The central margins on the anterior and posterior surfaces of the centrum are rounded. The level of the ventral margin of the anterior surface is dorsal to the level of the ventral margin of the posterior surface of the centrum, making the ventral margin slope posteroventrally, similar to *Pulanesaura* (BP/1/6201) but differing from the horizontal margin in *Melanorosaurus* (Galton *et al*. 2005). The ventral margin of the centrum is deeply concave with a weakly developed ventral keel. The presence of chevron facets cannot be determined due to the extent of the weathering.

Scapula

The left scapula of BP/1/8489 is the only pectoral girdle element preserved (Fig. 6). While nearly complete, its margins and cortical surface are poorly preserved. For the anatomical descriptions, the scapula will be oriented so that the blade is directed dorsally. The scapula is tall, with an anteroposteriorly short scapular shaft and an

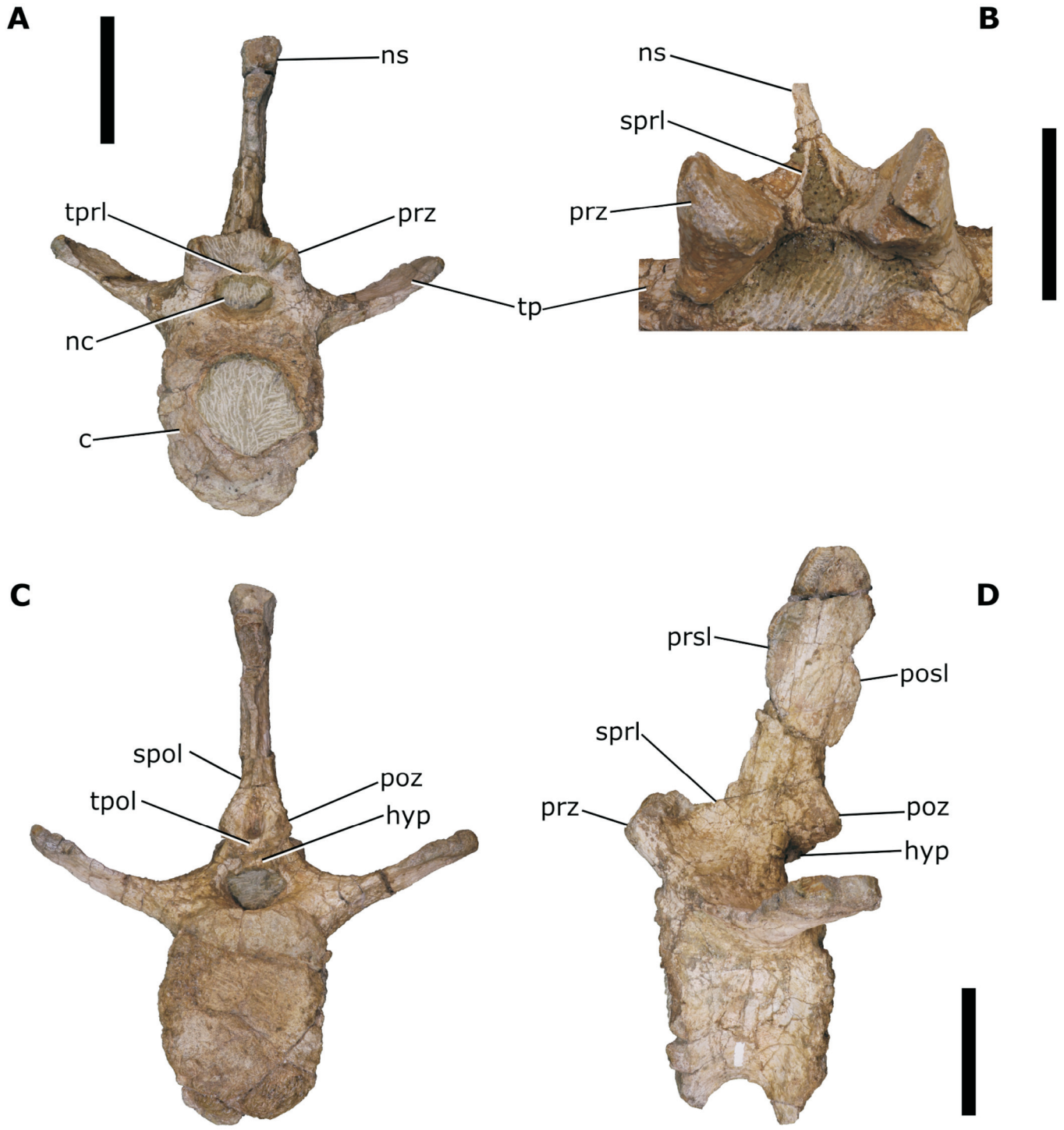

Figure 5. Anterior caudal vertebra of BP/1/8489. **A**, anterior; **B**, an enlargement of the sprl from another caudal vertebra; **C**, posterior; and **D**, left lateral views. Abbreviations: c, centrum; hyp, hyposphene; nc, neural canal; ns, neural spine; posl, postspinal lamina; poz, postzygapophyses; prsl, prespinal lamina; prz, prezygapophyses; spol, spinopostzygapophyseal lamina; sprl, spinoprezygapophyseal lamina; tp, transverse process; tpol, intrapostzygapophyseal lamina; tprl, intraprezygapophyseal lamina. Scale bar(s) equal: A, C, D, 10 cm; B, 5 cm.

anteroposteriorly long dorsal end. This is similar to those of *Antetonitrus* (BP/1/4952), *Lessemsaurus* (Pol & Powell 2007), *Kholumolumo* (Peyre de Fabrègues & Allain 2020), and *Yunnanosaurus* (Young 1942). It is also similar to *Sefapanosaurus* (BP/1/7433) with an anteroposteriorly short scapular shaft, but the dorsal end is not as expanded as in BP/1/8489. The minimum anteroposterior length of the scapula is approximately 0.21 times the dorsoventral height, but this ratio is overestimated given the incomplete length of the specimen. The ratio may be within the range of most sauropodomorphs with narrower scapular shafts such as *Melanorosaurus* (Galton *et al*. 2005), *Riojasaurus* (Bonaparte 1971), and *Massospondylus* (BP/1/4934).

The dorsal end is incomplete with the anterior expansion absent. The scapular blade is mediolaterally thin. The scapular blade projects strictly dorsally but is weakly concave along the anterior margin. The posterior margin of the dorsal end of the scapular blade extends beyond the posterior margin of the ventral end, creating a flange. The

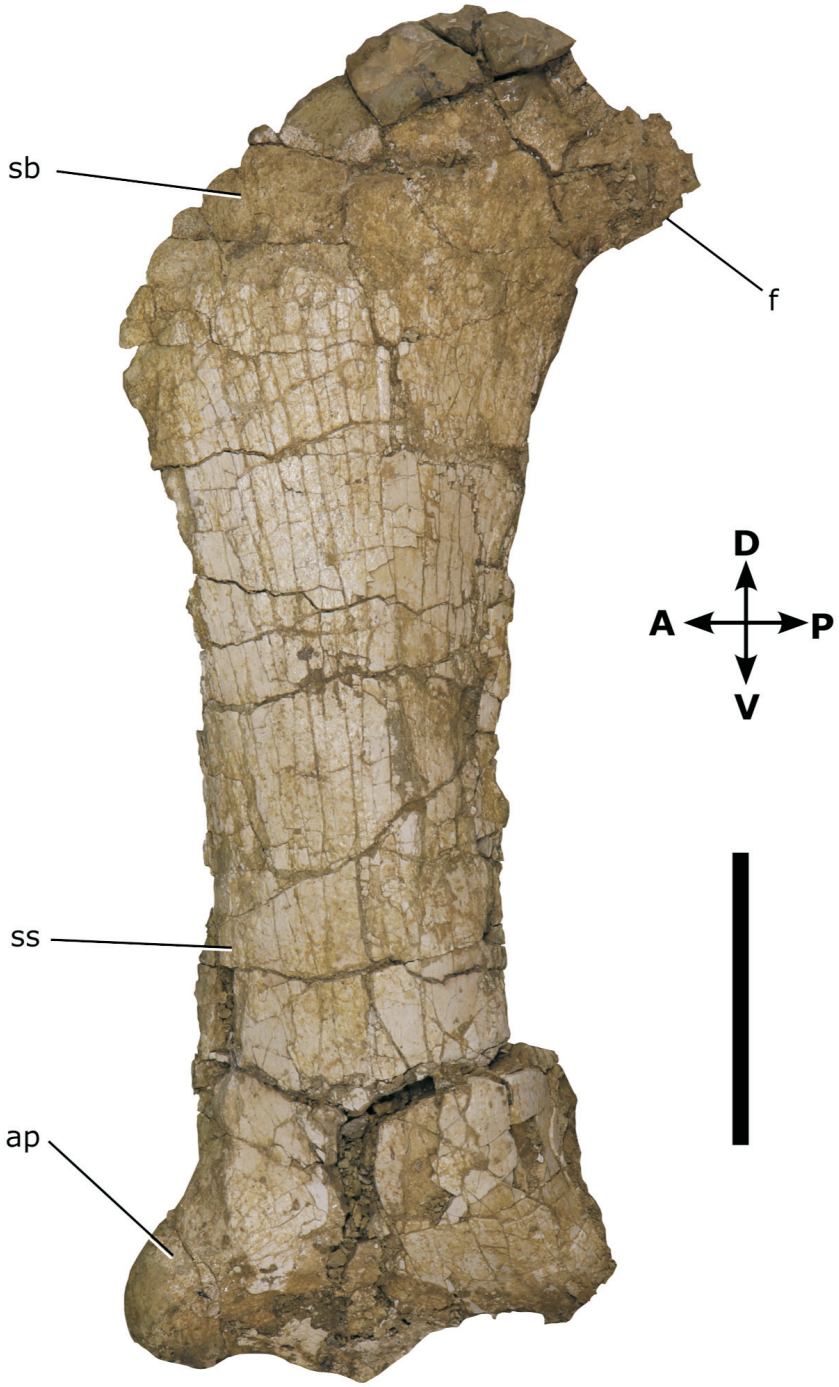

Figure 6. Lateral view of the left scapula of BP/1/8489. Abbreviations: ap, acromion process; f, flange; sb, scapular blade; ss, scapular shaft; A, anterior; D, dorsal; P, posterior; V, ventral. Scale bar = 10 cm.

flange is tall and short, forming a rounded posterior margin. This flange is also present in *Antetonitrus* (BP/1/4952) and *Lessemsaurus* (Pol & Powell 2007) but not in *Massospondylus* (BP/1/4934).

The ventral end of the scapula preserves the acromion region anteriorly but not the posterior region near the glenoid. The anteroposterior expansion of the acromial region appears to be less than that of the dorsal end, but due to the incomplete nature of the respective ends we cannot be certain. The dorsal margin of the acromion process is angled at approximately 35° from the longitudinal axis of the scapular blade, similar to the angles of *Antetonitrus* (BP/1/4952) and *Lessemsaurus* (Pol & Powell 2007).

Ilium

The preserved parts of the ilium consist of the postacetabular process of the right ilium and the left pubic peduncle (Fig. 7). Both of these portions of the ilium are well-preserved, with the dorsal margin of the postacetabular process slightly fragmented. These elements although isolated are sufficiently similar in size to have come from the same individual.

The postacetabular process is dorsoventrally low and anteroposteriorly long. Its dorsal margin is shallowly convex and is almost parallel to its longitudinal axis. The posterior margin of the postacetabular process is linear and nearly vertical with respect to the long axis, giving the posterior end a rectangular outline in lateral view. This is

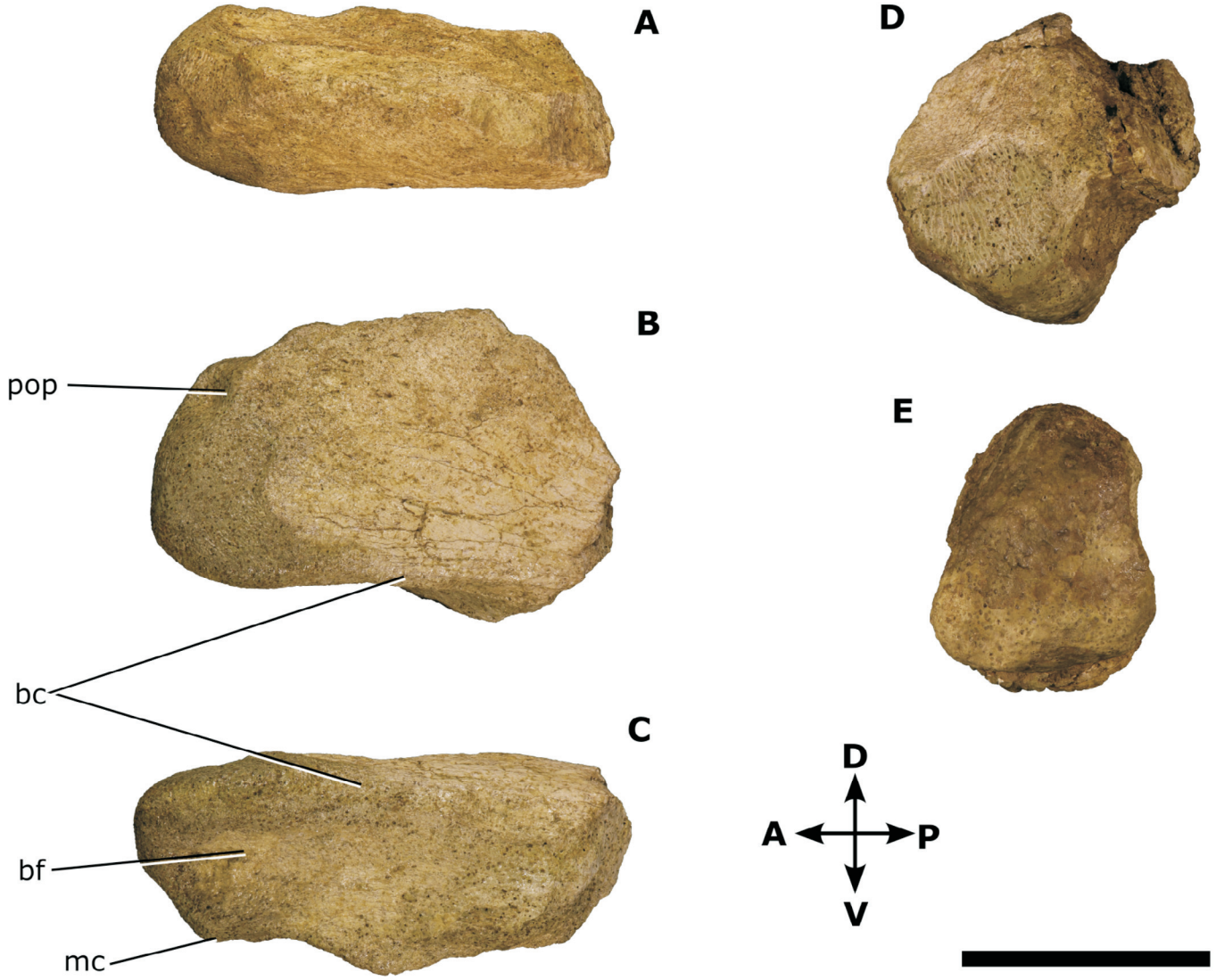

Figure 7. The right postacetabular process of BP/1/8489: **A**, dorsal; **B**, lateral; and **C**, ventral views. The left pubic peduncle of BP/1/8489: **D**, lateral; and **E**, ventral views. Abbreviations: bc, brevis crest; bf, brevis fossa; mc, medial crest; pop, postacetabular process. Directional: A, Anterior; D, dorsal; P, posterior; V, ventral. Scale bar = 10 cm.

similar to the ilia of *Antetonitrus* (BP/1/4952), *Riojasaurus* (Bonaparte 1971), and *Massospondylus* (BP/1/4934), whereas the posterior end of *Eucnemesaurus* (McPhee *et al*. 2015b) is subcircular in lateral view.

A well-developed brevis fossa with sharp medial and lateral margins is present on the ventral surface of the postacetabular process. The brevis fossa is longer than it is wide, maintaining its width for most of the area where it is developed. It is defined medially by the posterior extension of the brevis crest, which extends to form the ventromedial margin of the postacetabular process, as seen in *Eucnemesaurus* (McPhee *et al*. 2015b) and *Lessemsaurus* (Pol & Powell 2007). The brevis fossa is shallow from the anterior end and becomes slightly deeper towards the posterior end. The brevis fossa occupies the majority of the ventral margin of the postacetabular blade, similar to that of *Eucnemesaurus* (BP/1/6234) but differs markedly to the shorter brevis fossa in *Massospondylus* (BP/1/4934), whereas *Meroktenos* (Peyre de Fabrègues & Allain 2016) and *Kholumolumo* (Peyre de Fabrègues & Allain 2020) lack a brevis fossa altogether.

The left pubic peduncle is triangular in cross-section and rectangular in lateral view. The anterior margin of the pubic peduncle is convex and the posterior margin is concave, as is typical for early branching sauropodomorphs. The medial margin is rounded and relatively flat in comparison to many other sauropodomorphs (e.g. NMQR 1551) that display a sharp, protruding medial margin.

Femur

A nearly complete right femur and left femoral head are associated with BP/1/8489 (Fig. 8). During preparation, the right femur was left partially embedded within mudstone because of its fragile condition, and its posterior surface is severely fragmented, preserving little anatomical detail. The anterior surface of the femoral shaft is also highly fragmented, but as the femoral head and distal condyles are well-preserved with little damage or weathering, this will form the basis of the following description. The femur is very large and gracile. The femur is weakly sigmoidal in lateral and anterior view with the distal end directed posteriorly, similarly to *Lessemsaurus* (Pol & Powell 2007). In *Meroktenos* (Peyre de Fabrègues & Allain 2016) and

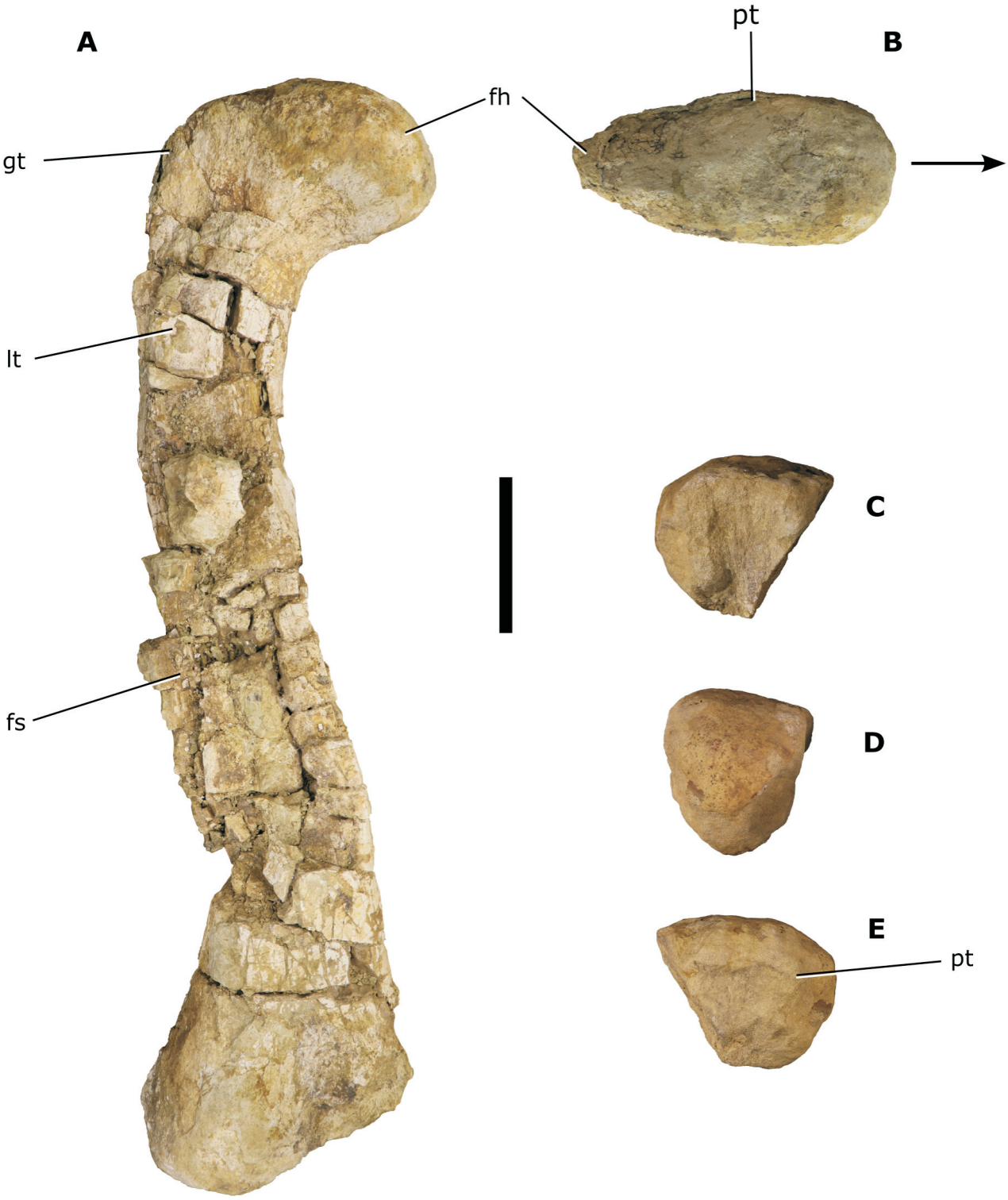

Figure 8. The right femur of BP/1/8489: **A**, anterior; **B**, dorsal view with the arrow directed medially. The left femoral head: **C**, anterior; **D**, medial; and **E**, posterior views. Abbreviations: fh, femoral head; fs, femoral shaft; gt, greater trochanter; lt, lesser trochanter; pt, posterior tubercle. Scale bar = 10 cm.

Kholumolumo (Peyre de Fabrègues & Allain 2020) the femur is straight with the distal end directed posteriorly.

The femoral head is well developed and medially inturned. Its long axis is sub-perpendicular to the longitudinal axis of the femur and in proximal view, this axis is deflected anteriorly similar to that of *Antetonitrus* (BP/1/4952) with an approximate angle of 20°. The femoral head is subrectangular in medial view with a sharp posterodorsal corner. A small swelling is present on the mesial portion of the proximal end of posterior surface of the femoral head and we identify it here as homologous to the posterior tubercle present in *Eucnemesaurus* (BP/1/6234), *Lessemsaurus* (Pol & Powell 2007), and possibly *Kholumolumo* (Peyre de Fabrègues & Allain 2020). The cortical bone on the distal margin of the femoral head is compressed resulting in an artificially concave margin. The lateral margin of the femoral head has a thick ridge suggesting the presence of a greater trochanter that follows the lateral margin of the femoral shaft.

Only the proximal portion of the lesser trochanter is

preserved. The lesser trochanter is located along the midline of the long axis of the anterior surface of the femoral shaft, whereas in *Antetonitrus* (BP/1/4952) and *Mussaurus* (Otero & Pol 2013) it is positioned more laterally. It is proximodistally orientated as a well-developed, elongate ridge projecting as a raised process. The proximal portion of the lesser trochanter begins in step with the distal margin of the femoral head and rises from the femoral shaft at a gradual slope.

The femoral shaft is estimated to be elliptical in cross-section, being slighter wider than it is long, similar to that of *Eucnemesaurus* (BP/1/6234). Although broken, its cross-sectional geometry appears intermediate between the subcircular femoral shafts of early branching sauropodomorphs (e.g. *Aardonyx*, *Ledumahadi*, *Mussaurus*, *Kholumolumo*) and the more elliptical femoral shafts of later diverging sauropodomorphs (e.g. *Antetonitrus*, *Meroktenos*), i.e. it is subovoid. The distal end of the femur is mediolaterally expanded at the level of the condyles relative to the width of the femoral shaft. A shallow extensor depression is present on the anterior surface of the distal end of the femur and is centrally located, similar to that of *Antetonitrus* (BP/1/4952) but differs compared to the more well-developed depression in *Mussaurus* (Otero & Pol 2013).

Phalanges

Two phalanges are preserved that are associated with BP/1/8489 (Fig. 9). Both of the phalanges cannot be confidently assigned to the manus or pes, but based on their proportions they belong to one individual. The first phalanx (Fig. 9A–C) described is likely from the manus and possibly from digit I based on the strongly convex ventral surface and the distally angled proximal surface. The phalanx lacks the distal condyles. The proximal articulation surface is relatively intact with a quadrangular, concave surface that is wider than it is tall. The proximal dorsal surface of the phalanx is slightly concave and gradually becomes convex towards the distal end, and the ventral surface of the phalanx is concave.

The second phalanx (Fig. 9D–G) preserved is likely a distal pedal phalanx based on its flat ventral surface. It is proximodistally longer than it is mediolaterally wide, with a constriction at the midpoint. The proximal articulation surface is missing the dorsal portion of the articulation and the ventral portion of the articulation that is present, suggests a concave surface. The intercondylar groove on the proximal articulation is not prominent but is present. The distal articulation is trapezoidal in distal view with the dorsal margin narrower than the ventral margin. There are well-developed condyles with deep collateral fossae on the phalanx. The dorsal surface of the phalanx is relatively flat with the ventral surface becoming concave distally.

Ungual

One ungual is preserved, and is only missing the distal tip (Fig. 9H–K). It is likely a pedal ungual from a lateral digit based on its flat ventral surface, its dorsoventral flattening, and its asymmetry. The ungual is proximo-

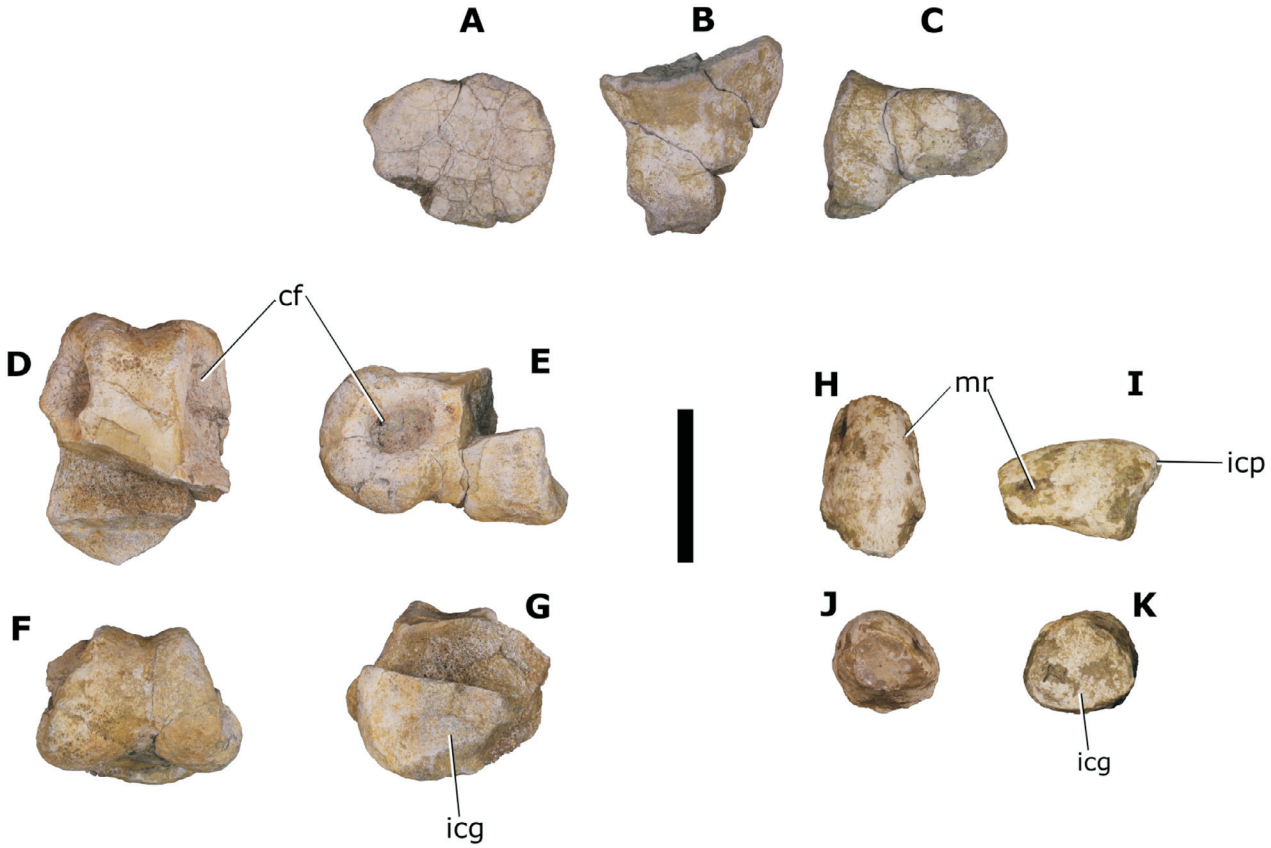

Figure 9. Phalanges and ungual of BP/1/8489. The manual phalanx: **A**, proximal; **B**, dorsal; and **C**, lateral views. The pedal phalanx: **D**, dorsal; **E**, lateral; **F**, distal; and **G**, proximal views. The ungual: **H**, dorsal; **I**, lateral; **J**, distal; and **K**, proximal views. Abbreviations: cf, collateral fossa; icg, intercondylar groove; icp, intercondylar process; mr, medial ridge. Scale bar = 5 cm.

distally longer than it is wide. Distinct ridges for the attachment of the ungual sheath are visible on both sides. The dorsal and ventral margins of the ungual curve slightly downwards. The dorsal surface has its apex directed laterally with the ventral surface being flat resulting in a triangular ungual in proximal view. As the apex of the dorsal surface is directed laterally, it creates an asymmetrical ungual similar to that of *Lessemsaurus* (Pol & Powell 2007) which differs markedly to the vertically oriented unguals of *Mussaurus* (Otero & Pol 2013) and *Pulanesaura* (BP/1/6186). The proximal articulation surface is smooth with the presence of an intercondylar groove and a small dorsal intercondylar process present.

Description of plant material

Cycadopsida Brongniart, 1843
Phasmatocycadales Doweld, 2001
Phasmatocycadaceae Doweld, 2001
Taeniopteris Brongniart, 1828

cf. *Taeniopteris homerifolius* Anderson & Anderson, 1989

Two specimens (Fig. 10A,H) are confidently referred to this type and are represented by minimally fragmented impressions. Most specimens were fragmented with the medial portion of the leaves preserved (Fig. 10A,F,H). Taeniopterids are challenging to group, since several major groups of plants could potentially be assigned to *Taeniopteris*. Taxa placed in *Taeniopteris* include ferns, cycads, bennettitaleans, and pentoxylaleans. Sterile leaves with an entire margin that may or may not bifurcate at the midrib are grouped under taeniopterids (van Konijnenburg-van Cittert *et al*. 2017). These include leaves from *Taeniopteris*, *Nilssoniopteris*, and *Nilssonia* amongst others. This typification of impression leaf fossils is broad and has long been debated amongst researchers (see Kvaček & Straková 1997; Cleal & Rees 2003). Without the presence of attached fertile structures or cuticular structures, venation type and leaf shape are the only morphological features that are currently used to differentiate between and within the genera (Anderson *et al*. 1998; van Konijnenburg-van Cittert *et al*. 2017). The emended diagnosis of *Taeniopteris* is 'Leaves with a simple, entire-margined lamina. Midvein rigid, extending for entire length of leaf. Lateral veins approximately perpendicular to midvein, simple or forking at base. Evidence of epidermal structure not known' (Brongniart, 1828).

Description: simple leaf, small, with an entire margin. Shape elliptical to linear. Leaf width 14.46 mm and length 52.77 mm, these measurements are based on the most complete leaf. Apex is acute with an angle of approximately 82.38° and base absent (Fig. 10A). Secondary veins bifurcate occasionally mid-lamina towards the margin; the medial vein angle proximal at the midrib (64.51–74.39°) increases towards the margin (72.43–76.67°).

Filicopsida C. Agardh, 1822
? Osmundales Berchtold & J. Presl, 1820
Osmundaceae Berchtold & J. Presl, 1820
Cladophlebis Brongniart, 1849

cf. *Cladophlebis janetae* Anderson & Anderson, 2008

Anderson & Anderson (2008) placed most fern sterile fronds under the order ?Osmundales. The same genus also has intraspecies and interspecies variation making the frond almost impossible to identify. The fronds are difficult to distinguish without attached reproductive material such as sporangia. cf. *Cladophlebis janetae* (Fig. 10C) sterile foliage could be associated with the fertile foliage of *Rooitodites integra* (Anderson & Anderson 2008).

Description: sterile fond; length ≈26 mm. Frond bipinnate; lobed; pinnules opposite, 6 on the left and 5 on the right. Several pinnules are contracted at the base. Midrib present on pinnules. Lateral veins on pinnules are poorly preserved.

Incertae sedis *plant fossils*

These specimens could not be placed into definite taxa as they were poorly preserved and lacked conclusive identifying features. Figures 10E and 10G resemble fern pinnules on a fine matrix, which is favourable for ferns to preserve because of their delicate tissue. Figure 10E could also be a twig based on the general morphology of a stem and faint lateral branches. The faint lateral branches are probably an artefact of preservation. These specimens add to the general diversity of this collection. With further bulk collections, more detailed and probably complete specimens can be found to improve these specimens' identification and taxonomic placement.

Description of plant–insect interactions

Damage types observed on these plant fossils include margin feeding (DT 12 and DT 15; Fig. 10B) and ovipositions (DT 76; Fig. 10D). All damage types were identified using Labandeira *et al*. (2007). These are the first conclusive insect damage classification from the lower Elliot Formation. The excellent record of insect-leaf damage and insect body fossils from the Molteno (see Anderson *et al*. 1998; Labandeira *et al*. 2018) has led some researchers to speculate about the fauna of the lEF (Anderson *et al*. 1998; Scott *et al*. 2004). Our observations suggest that the lEF, although not conformable with the Molteno, preserves similar suites of species.

PHYLOGENETIC ANALYSIS

The maximum parsimony (MP) analysis using the character matrix from McPhee *et al*. (2018) resulted in six most parsimonious trees (MPTs) with a tree length of 1291 steps (Fig. 11). These trees have a consistency index (CI) of 0.34 and a retention index (RI) of 0.68. The MP analysis using the character matrix from Pol *et al*. (2021a) resulted in 1175 MPTs with a tree length of 1608 steps (Fig. 12). These trees have a CI of 0.36 and a RI of 0.62. Bremer supports are relatively low for both of the datasets ranging from one for majority of the nodes to three and four near the base of Sauropoda. Bootstrap supports are also relatively low with majority of the nodes below 50% for both datasets, and a few ranging up to 82% e.g. *Efraasia* + Plateosauria (Fig. 11), and 64% for *Pantydraco* + *Thecodontosaurus* (Fig. 12).

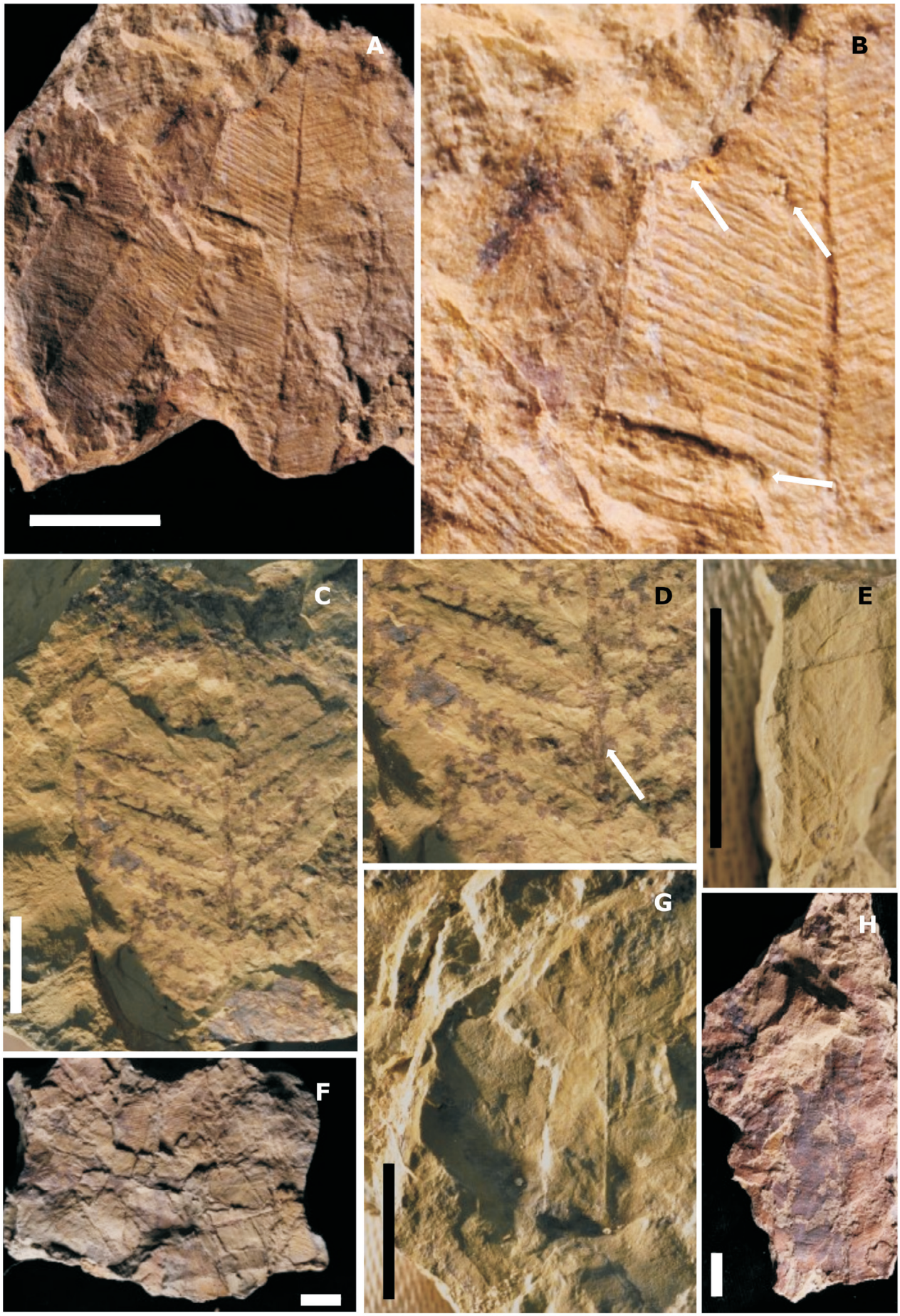

Figure 10. Plant fossils of the lower Elliot Formation. **A**, cf. *Taeniopteris homerifolius* leaves; **B**, cf. *Taeniopteris* leaves with external insect foliage feeding (DT 12 and DT 15) in the apical region and extending almost towards the midrib; **C**, cf. *Cladophlebis janetae*; **D**, cf. *Cladophlebis janetae* with DT 76; **E** and **G**, *incertae sedis* plant fossils of the lEF; **F** and **H**, slabs with fragmented *Taeniopteris* leaves. Scale bar = 1 cm.

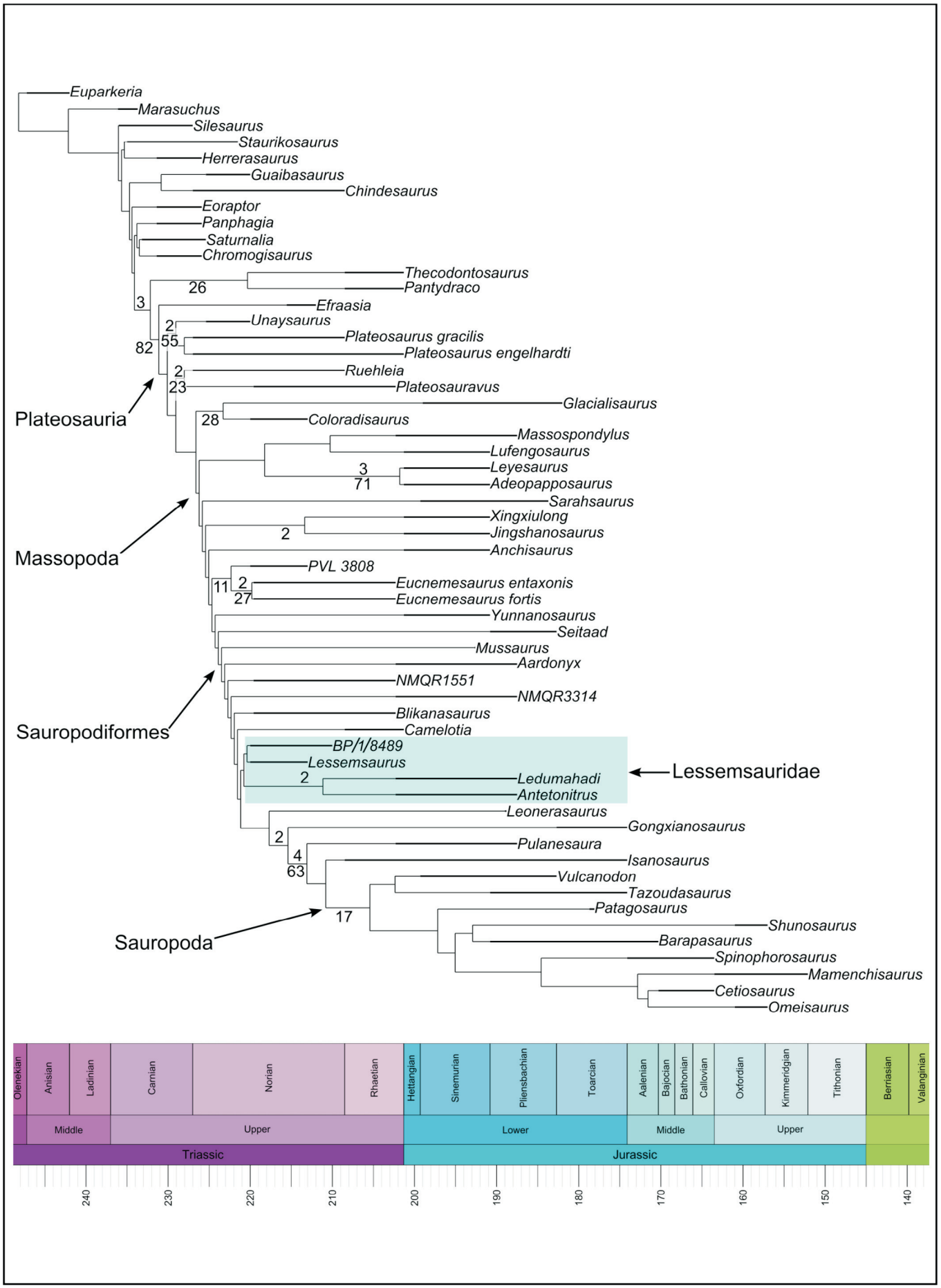

Figure 11. Time-calibrated phylogeny depicting the position of BP/1/8489 in the McPhee *et al.* (2018) dataset. The numbers above the nodes represent Bremer support and numbers below represent Bootstrap support.

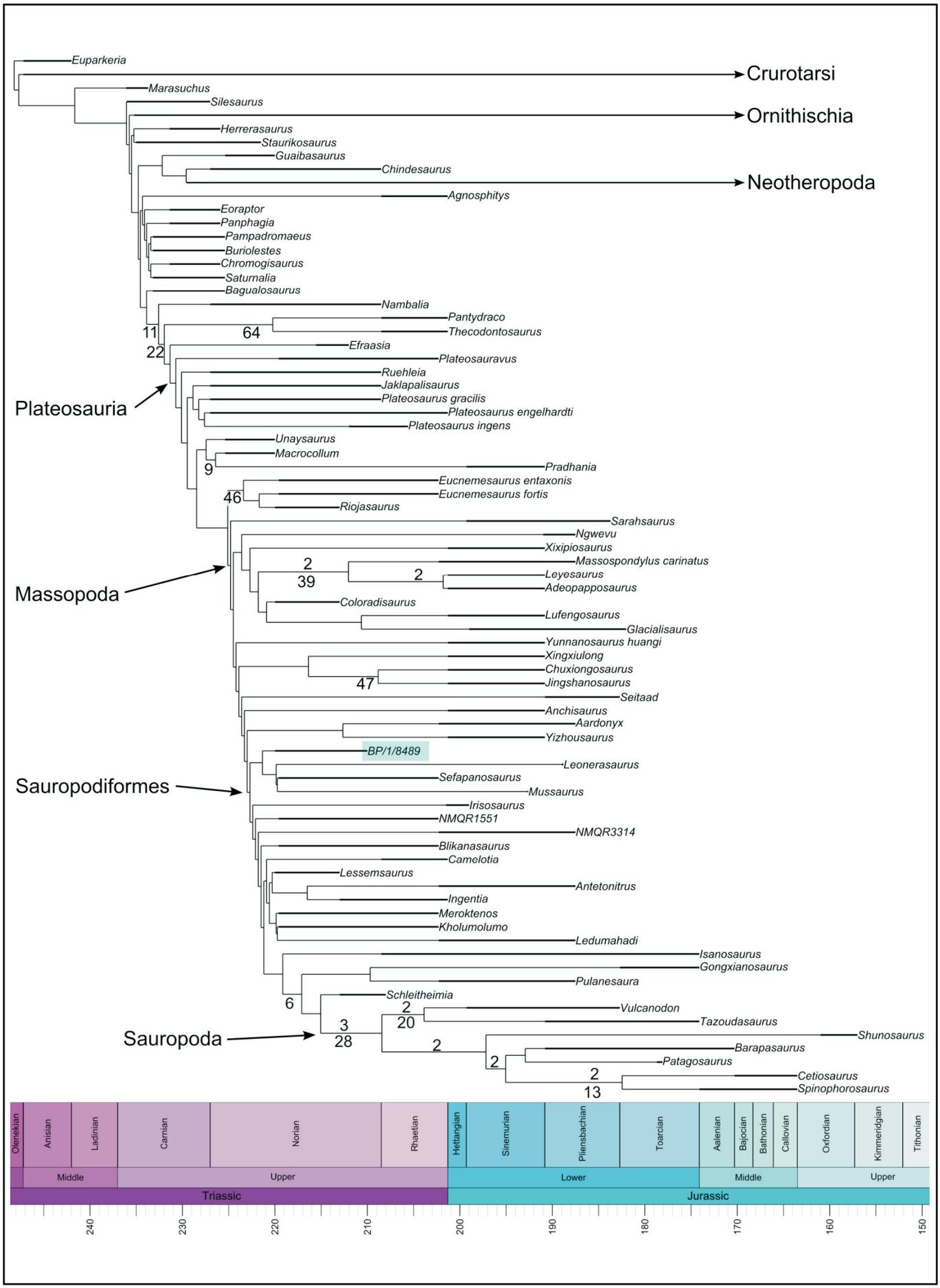

Figure 12. Time-calibrated phylogeny depicting the position of BP/1/8489 in the Pol *et al.* (2021) dataset. The numbers above the nodes represent Bremer support and numbers below represent Bootstrap support.

BP/1/8489 is recovered as a lessemsaurid within McPhee *et al*. (2018, Fig. 11), whereas in Pol *et al*. (2021a; Fig. 12) it is placed as a basal sauropodiform. The results of the implied weighting analyses on the Pol *et al*. (2021a) dataset places BP/1/8489 amongst Lessemsauridae (see S1) similarly to McPhee *et al*. (2018), however, it differs by forming a clade with *Meroktenos*, *Kholumolumo*, and *Ledumahadi*. Constrained analyses forcing a lessemsaurid affinity for BP/1/8489 in Pol *et al*. (2021a) dataset result in a tree length of 1609 steps (see S1), one stop longer than the unconstrained parsimony analysis, and with similar relationships to the unconstrained analysis of the McPhee *et al*. (2018) dataset.

Within the McPhee *et al*. (2018) dataset, BP/1/8489 is placed within Lessemsauridae as a sister taxon to *Lessemsaurus*. This node is supported by the following synapomorphies: angle between the long axis of the femoral head; the transverse axis of the distal femur is about 30 degrees; and the lesser trochanter is not visible in posterior view. Both of these characters are, however, plesiomorphic with a distribution amongst many early branching sauropodomorphs, i.e. they are highly homoplastic in early branching sauropodomorphs. Characters supporting BP/1/8489 within Lessemsauridae include: the shape of the anterior dorsal neural spines; minimum width of the scapula; and width of the dorsal expansion of the scapula. The shape of the dorsal neural spines is a homoplastic feature that is present in *Plateosauravus*, *Ruehleia*, *Yunnanosaurus*, *Antetonitrus*, *Ledumahadi*, and *Lessemsaurus*. The width of the scapula is almost exclusively a lessemsaurid feature, but outside of lessemsaurids it is also present in *Jingshanosaurus* and *Xingxiulong*. The width of the dorsal expansion of the scapula appears as an exclusively lessemsaurid feature.

In the Pol *et al*. (2021a) dataset, BP/1/8489 forms a clade with *Leonerasaurus*, *Sefapanosaurus*, and *Mussaurus* at the base of Sauropodiformes. This clade is supported by: the length of the base of the proximal caudal neural spines; and a well-developed brevis fossa with sharp margins on the ventral surface of the postacetabular process of the ilium. Both of these characters are plesiomorphic for sauropodiforms, but have high homoplasy and are sparsely distributed across early branching sauropodomorphs. After applying implied weighting, BP/1/8489 forms a clade with *Meroktenos*, *Kholumolumo*, and *Ledumahadi*. This is supported by: the position of the lesser trochanter; and the visibility of the lesser trochanter in posterior view. Both of these characters are plesiomorphic and are present in all lessemsaurids, with the exception of *Antetonitrus*. The constrained analysis that resulted with BP/1/8489 within Lessemsauridae is supported by the same characters as the implied weighting.

Synapomorphies between BP/1/8489 and other lessemsaurids include: the dorsal neural spine bowing posteriorly; the dorsal neural spine widens laterally as it extends dorsally; and the minimum width of the scapula is greater than 20% of its length. Together with *Lessemsaurus* and *Antetonitrus*, BP/1/8489 shares a scapula with a flange on the posterior margin of the distal end and an acromion process that rises at a similar angle from the scapular shaft. While other lessemsaurids such as *Lessemsaurus* and *Antetonitrus* have a strong distal scapular expansion, the poor preservation of the anterior region of the distal end of the scapula in BP/1/8489 prevents full comparison. BP/1/8489 shares a procoelous anterior caudal with a deep, concave anterior face and a shallow, convex posterior face with *Ledumahadi* (McPhee *et al*. 2018).

While the fragmentary nature of the specimen makes comparisons challenging, several salient features of the anatomy are unique to BP/1/8489 or at least to its region of the sauropodomorph tree. These include: a sheet-like centropostzygapophyseal lamina on the anterior dorsal commonly seen in later-branching sauropodomorphs such as the lessemsaurid *Antetonitrus* (McPhee *et al*. 2014) and the early sauropod *Tazoudasaurus* (Allain & Aquesbi 2008); the postzygapophyseal articular facets on the posterior dorsal are anteroposteriorly long ellipses, present in *Ledumahadi* (McPhee *et al*. 2018) and *Pulanesaura* (McPhee *et al*. 2015a) but few other sauropodomorphs; a pocdf with subsidiary fossae in the posterior dorsal are seen in later-branching sauropodomorphs such as *Antetonitrus* (McPhee *et al*. 2014) and *Pulanesaura* (McPhee *et al*. 2015a), but incipient subsidiary fossae are possibly present in the early branching sauropodomorphs *Plateosaurus* (Moser 2003) and *Massospondylus* (Barrett *et al*. 2019); dorsally curving transverse processes in the anterior caudal, currently only known in *Pulanesaura* (McPhee *et al*. 2015a); a posterior flange on the distal end of the scapula, currently considered to be a synapomorphy for lessemsaurids; a well-developed, ventrally facing brevis fossa with sharp margins is a variable feature that occurs across many sauropodomorphs including *Plateosaurus* (Moser 2003) and *Mussaurus* (Otero & Pol 2013); a well-developed posterior tubercle on the femoral head, notably present also in Riojasauridae; and the lesser trochanter positioned along the midline of the femoral shaft is homoplastically distributed among many non-sauropodan sauropodomorphs. The femoral length might be locally important but cannot be autapomorphic, in addition this is not a mature individual resulting in length as an unsuitable character for assessing relationships.

BP/1/8489 also possesses characters that are plesiomorphic for Sauropodomorpha that include: the absence of spinodiapophyseal lamina on the dorsal vertebrae; a narrow scapular shaft; an ilium with a straight dorsal margin based on the postacetabular process; the distal end of the femur is posteriorly bent and is weakly sigmoid. Other features observed in BP/1/8489 are derived characters that are generally present in sauropods and include: high neural arches in the dorsal vertebrae; the well-developed spinopostzygapophyseal lamina; anteroposteriorly short anterior caudal vertebrae; and the ventral surface of the pedal ungual is flattened, all of which are also present in the lessemsaurid *Ledumahadi* (McPhee *et al*. 2018).

BODY MASS ESTIMATION

Mediolateral diameter and minimum shaft circumference are strongly correlated in sauropodomorphs

(Fig. 13), with a generalized least squares regression coefficient of 0.9898 with no large outliers amongst the data we collated. The regression equation for estimating the femoral circumference from mediolateral shaft diameter based on this analysis is as follows:

$$Log_{10}FC = 0.8891 \cdot Log_{10}FML + 0.677$$

The femoral circumference of BP/1/8489 was estimated at 305.43 mm using a diameter of 108 mm. Using this estimated femoral circumference, the quadrupedal mass equation (Table 2) estimates BP/1/8489 at 3.85 metric tons with a standard error of 0.175, and the bipedal mass equation (Table 2) estimating it at 1.45 metric tons with a standard error of 0.241.

DISCUSSION

Stratigraphic positions of sauropodomorphs from the lower Elliot Formation

BP/1/8489 is among the stratigraphically lowest, and thus oldest, sauropodomorphs from the lower Elliot Formation (lEF), provenanced at the base of the lEF approximately 20 m above the contact with the underlying Molteno Formation. The oldest strata in the lEF to be reliably dated are tuffaceous layers from the northern part of the basin, which have a minimum depositional age of at least 218 Ma (Bordy *et al*. 2020). Although these well-dated strata are approximately 300 km from the Rossouw locality, we assume they are approximately correlative in their relative position to the Molteno and overlying EF deposits. This indicates that BP/1/8489 lived during the mid-Norian, alongside other lEF taxa like *Scalenodontoides*, *Blikanasaurus*, *Eucnemesaurus*, *Meroktenos*, *Kholumolumo*, *Plateosauravus*, and *Melanorosaurus* (McPhee *et al*. 2017; Viglietti *et al*. 2020b), and was a contemporary of Argentinian sauropodomorphs such as *Coloradisaurus*, *Ingentia*, *Lessemsaurus*, and *Riojasaurus* (Pol *et al*. 2021b).

Previously described sauropodomorph taxa with stratigraphic positions similar to BP/1/8489 in the lEF include *Plateosauravus* (15 m above the lEF/Molteno boundary), *Eucnemesaurus fortis* (55 m above the boundary), *Melanorosaurus* (120 m above the boundary), and *Blikanasaurus* (50 m above the boundary; McPhee *et al*. 2017). *Meroktenos* and *Kholumolumo* are provenanced within the lEF but their stratigraphic positions are less clear, although *Kholumolumo* is likely closer to the uEF/lEF boundary based on the position of the Maphutseng quarry (Bordy *et al*. 2020). Of these taxa, BP/1/8489 can be readily differentiated from *Plateosauravus*, *Eucnemesaurus entaxonis*, and *Melanorosaurus* based on the differing morphology of its femur and postzygapophyseal articular facets of dorsal vertebrae. These differences indicate that BP/1/8489 cannot be referred to any of these genera. There are no overlapping elements between BP/1/8489 and *Blikanasaurus*; however, *Blikanasaurus* appears to be a very robust animal and we note the gracility of the BP/1/8489 femur, which potentially suggests they represent different taxa. Some femoral features of BP/1/8489 are similar to those observed in

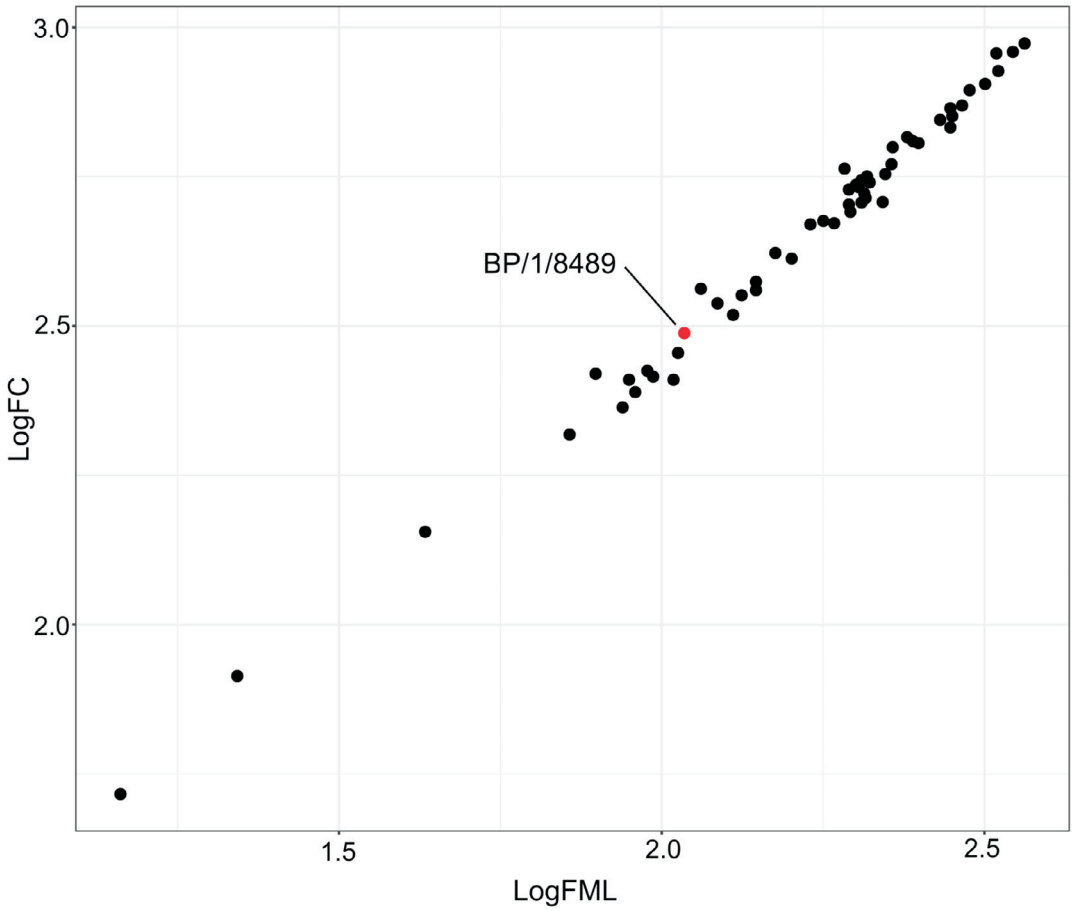

Figure 13. Relationship between between log_{10} femoral circumference and log_{10} mediolateral diameter femoral circumference and mediolateral diameter of the femoral shaft in sauropodomorphs. BP/1/8489 is indicated in red.

Meroktenos including the centrally located lesser trochanter and the lack of visibility of this trochanter in posterior view. In our phylogenetic analyses, these features are interpreted as synapomorphies of these taxa. Many similarities exist between *Kholumolumo* and BP/1/8489, such as the posteriorly directed neural spine of the caudal vertebrae, the overall scapular morphology, and the overall femoral morphology. However, *Kholumolumo* can be differentiated readily based on its much more robust dorsal vertebral lamination relative to BP/1/8489. In summary, no known lEF sauropodomorph taxon has a full suite of identical anatomical features when compared to BP/1/8489; because of this, we consider it likely to represent a previously unknown taxon until additional morphological information is available.

Phylogenetic affinities of BP/1/8489 and Lessemsauridae

Our phylogenetic analyses recover BP/1/8489 as either a basal sauropodiform or as a lessemsaurid, albeit with relatively weak support for either position due to the limited number of bones that are preserved. There are many synapomorphies between BP/1/8489 and other lessemsaurids such as: dorsal neural spine bowing posteriorly; the dorsal neural spine widens laterally as it extends dorsally; minimum width of the scapula is greater than 20% of its length; width of the dorsal expansion of the scapula is subequal to the ventral end, this is inferred for BP/1/8489; weakly sigmoidal femoral shaft; position of the lesser trochanter is near the centre of the anterior surface of the femoral shaft; and the lesser trochanter is not visible in posterior view.

While the phylogenetic results differ between the two matrices we used here, we note that in the equally weighted Pol *et al*. (2021a) dataset, hypotheses considering BP/1/8489 as a lessemsaurid are only one step longer than the most-parsimonious trees. Additionally, all sensitivity analyses using implied weighting recover lessemsaurid affinities for the specimen (Fig. 14). We therefore consider that the most likely position for BP/1/8489 is among Lessemsauridae, but acknowledge that additional morphological information is necessary to more rigorously test this hypothesis. This assessment provides an important point of biostratigraphic correlation between Norian deposits in Argentina, South Africa, and Lesotho. BP/1/8489 within Lessemsauridae supports that lessemsaurids were not experiencing geographic isolation prior to the onset of the end-Triassic extinction (Apaldetti *et al*. 2021).

The salient features of BP/1/8489 that are potentially autapomorphic include: the sheet-like centropostzygapophyseal laminae on the dorsal neural arch; the postzygapophyseal articular facets on the posterior dorsal are anteroposteriorly long ellipses; a postzygodiapophyseal fossa with subsidiary fossae in the posterior dorsal; and dorsally curving transverse processes in the anterior caudal. These features along with synapomorphies shared with other lessemsaurids support the later-branching position of BP/1/8489. Although we do not elect to formally name BP/1/8489 here, these potentially autapomorphic features will prove useful for diagnosis should a more complete specimen be found.

The well-developed laminations and fossae of the vertebrae are likely associated with body size as many larger-bodied sauropodomorphs and giant sauropods have these pronounced features, and it further supports incipient pneumatization within sauropodomorphs approaching Sauropoda (Benson *et al*. 2012; Yates *et al*. 2012). The dorsally concave, distally upturned transverse processes of the anterior caudal are not present in earlier-branching sauropodomorphs but are present in the later-branching sauropodomorph *Pulanesaura*. This character is not included in the morphological datasets as a character, and the phylogenetic utility and distribution of this feature should be investigated further. Novel morphologies that have been recently discovered will be systematically incorporated into future phylogenetic datasets, enabling us to improve our understanding on the evolutionary relationships within Sauropodomorpha.

Sauropodomorph body masses during the Norian

Regardless of the inferred posture of BP/1/8489, it is among the largest EF sauropodomorphs and provides confirmatory evidence that sauropodomorph body masses were increasing rapidly in the Norian. If BP/1/8489 was a biped, its estimated mass is 1.45 tonnes, making it comparable to the largest described bipedal sauropodomorphs like *Plateosauravus* (1.3 tonnes), *Mussaurus* (1.15 tonnes), and *Ruehleia* (1.14 tonnes; McPhee *et al*. 2018). Alternatively, if BP/1/8489 was quadrupedal, its estimated body mass of 3.85 tonnes is comparable to larger Norian sauropodomorphs like *Riojasaurus* (2.23 tonnes; Benson *et al*. 2017; Apaldetti *et al*. 2018; McPhee *et al*. 2018). This quadrupedal body size estimate is also comparable to that of *Kholumolumo* (3.2 tonnes; Peyre de Fabrègues & Allain 2020), which is considered here as a lessemsaurid. However, the poorly fused neural arches of BP/1/8489 suggest it is skeletally immature, and its adult body mass could have

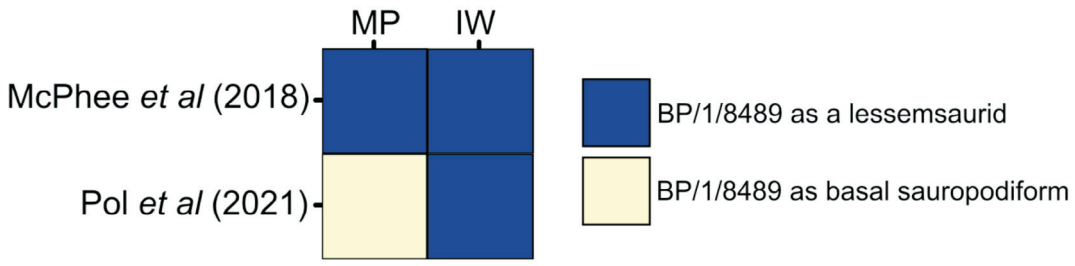

Figure 14. A comparison of BP/1/8489 phylogenetic position across the various phylogenies from the McPhee *et al.* (2018) and Pol *et al.* (2021) datasets. MP, Maximum parsimony; IW, implied weighting.

been somewhat larger, potentially making it similar in adult body mass to the lessemsaurid *Antetonitrus* (5.6 tonnes) and the estimated seven-tonne body mass of *Lessemsaurus* (Apaldetti *et al*. 2018). If BP/1/8489 was a biped, it would be the first representative of this posture known within Lessemsauridae. If it is a quadruped, its mid-Norian age and large size (with potentially even larger adult size) provides important confirmatory evidence that body size increases and postural changes in lessemsaurids must have been underway at that time (Apaldetti *et al*. 2021).

Plant–vertebrate co-occurrences in the Elliot Formation

The plant fossils described here are among the first leaf impressions from the EF, and they suggest a continuation of the *Dicroidium* flora from the Molteno. Their presence in association with BP/1/8489 provides the only documented EF plant–vertebrate co-occurrence and one of only a handful of dinosaur–plant co-occurrences worldwide (Barrett & Willis 2001; Butler *et al*. 2009; Sander *et al*. 2010; Barrett 2014). Although the preservation of cf. *Taeniopteris* and *Cladophlebis* leaves with BP/1/8489 does not indicate foraging behavior, it does confirm that sauropodomorphs were at least living amongst such vegetation types.

In South African stratigraphy, *Taeniopteris* and *Cladophlebis* have been documented in the underlying Molteno Formation (Late Triassic; Anderson *et al*. 1998; Scott *et al*. 2004). The *Cladophlebis* species in the EF also occurs in the Molteno, but is different from the *Cladophlebis* species documented in the Burgersdorp Formation (Middle Triassic; Hancox *et al*. 2020). Both of these genera are widespread globally, with similar distributions in the Triassic. The insect damage types (Fig. 10B,D) appear similar to the underlying Molteno specimens and therefore support the hypothesis by Plumstead (1969) that the EF flora (and its associated fauna) would be continuations of the *Dicroidium* flora that is widely represented in the Triassic, and likely represents an open woodland habitat type.

CONCLUSION

BP/1/8489 is considered here as a possible lessemsaurid from the mid Norian (lEF) of South Africa with a geological age of approximately 218 Ma. This sauropodomorph displays a unique combination of plesiomorphic and autapomorphic characters. Although the posture of BP/1/8489 is unknown, body mass estimates as a biped and quadruped make this specimen one of the largest sauropodomorphs during the Norian, even though the individual has not reached adult body size. BP/1/8489 contributes to the already depauperate lEF as one of the stratigraphically lowest sauropodomorph body fossils and allows the lEF to be more comparable to other contemporaneous taxa. The gracility of BP/1/8489 in comparison to other lessemsaurids and early Norian taxa proposes that the early Norian is a critical time for body size experimentation within Sauropodomorpha. *Taeniopteris* and *Cladophlebis* preserved alongside this sauropodomorph documents one of the first co-occurrences of dinosaurs and plant material in the EF, as well as presents direct evidence of plant–insect herbivory from the lEF. The presence of a dinosaur body fossil, various plant morphotypes, and the evidence of plant–insect interactions provides some insight into the palaeoenvironment during the Late Triassic.

§ORCID iDs

A. Moopen: orcid.org/0000-0002-8420-0194
A. Matiwane: orcid.org/0000-0002-8841-0623
P.A. Viglietti: orcid.org/0000-0003-0102-5632
J.N. Choiniere: orcid.org/0000-0002-1008-0687

We thank B. Zipfel and S. Jirah for assisting in the collections. Thank you to Richard, Maryna, and Louise Roussouw, to Ben Maclennan, Gillian Warren-Brown, Hannie and Nellie van Heerden, Gerard Schmit, James Neenan, Blair W. McPhee, Kathleen Dollman, Cebisa Mdekazi, Kimberley E.J. Chapelle, Cory M. Dinter, Stephan Spiekman, and Gilbert Mokgoatha who collected and prepared the specimen. Thank you to Heidi Holmes for assisting with the plant identification of one of our leaves. Funding for this research was provided by the National Research Foundation (NRF) of South Africa and GENUS (DSI-NRF Centre of Excellence in Palaeosciences; GUN No. 127208), as well as DSI-NRF AOP grants awarded to J.N. Choiniere (GUN No. 98800, 118794, 136516). Funding for this research was also awarded to Pia A. Viglietti from GENUS (COE-2017, 2018) DST-NRF (project code: VIGL022), and Field Museum of Natural History's Grainger Bioinformatics Center.

REFERENCES

AGARDH, C.A. 1822. *Aphorismi botanici* **8**, 103–118.

ALLAIN, R. & AQUESBI, N. 2008. Anatomy and phylogenetic relationships of *Tazoudasaurus naimi* (Dinosauria, Sauropoda) from the late Early Jurassic of Morocco. *Geodiversitas* **30**(2), 345–424.

ANDERSON, H.M. & ANDERSON, J.M. 2008. *Molteno Ferns: Late Triassic Biodiversity in Southern Africa*. Pretoria, South African National Biodiversity Institute. 258 pp.

ANDERSON, J., HALL-MARTIN, A. & RUSSELL, D. 1985. Long-bone circumference and weight in mammals, birds and dinosaurs. *Journal of Zoology* **207**(1), 53–61.

ANDERSON, J.M. & ANDERSON, H.M. 1985. *Palaeoflora of Southern Africa: Prodromus of South African Megafloras Devonian to Lower Cretaceous*. Rotterdam, Balkema.

ANDERSON, J.M. & ANDERSON, H.M. 1989. *Palaeoflora of Southern Africa, Molteno Formation (Triassic). Gymnosperms (excluding* Dicroidium). Rotterdam, AA Balkema.

ANDERSON, J.M., ANDERSON, H.M. & CRUICKSHANK, A.R.I. 1998. Late Triassic ecosystems of the Molteno/Lower Elliot biome of southern Africa. *Palaeontology* **41**(3), 387–421.

APALDETTI, C. & MARTÍNEZ, R.N. 2022. South American non-Gravisaurian Sauropodiformes and the early trend towards gigantism. *South American Sauropodomorph Dinosaurs: Record, Diversity and Evolution*, 93–130.

APALDETTI, C., MARTÍNEZ, R.N., CERDA, I.A., POL, D. & ALCOBER, O. 2018. An early trend towards gigantism in Triassic sauropodomorph dinosaurs. *Nature Ecology & Evolution* **2**(8), 1227.

APALDETTI, C., POL, D., EZCURRA, M.D. & MARTÍNEZ, R.N. 2021. Sauropodomorph evolution across the Triassic–Jurassic boundary: body size, locomotion, and their influence on morphological disparity. *Scientific Reports* **11**(1), 22534.

BARRETT, P.M. 2014. Paleobiology of herbivorous dinosaurs. *Annual Review of Earth and Planetary Sciences* **42**, 207–230.

BARRETT, P.M., CHAPELLE, K.E., STAUNTON, C.K., BOTHA, J. & CHOINIERE, J.N. 2019. Postcranial osteology of the neotype specimen of *Massospondylus carinatus* Owen, 1854 (Dinosauria: Sauropodomorpha) from the upper Elliot formation of South Africa. *Palaentologia africana* **53**, 114–178.

BARRETT, P.M. & WILLIS, K.J. 2001. Did dinosaurs invent flowers? Dinosaur–angiosperm coevolution revisited. *Biological Reviews* **76**(3), 411–447.

BELL, M.A. & LLOYD, G.T., 2015. strap: an R package for plotting phylogenies against stratigraphy and assessing their stratigraphic congruence. *Palaeontology* **58**, 379–389.

BENSON, R.B., BUTLER, R.J., CARRANO, M.T. & O'CONNOR, P.M. 2012. Air-filled postcranial bones in theropod dinosaurs: physiological implications and the 'reptile'–bird transition. *Biological Reviews* **87**(1), 168–193.

BENSON, R.B., CAMPIONE, N.E., CARRANO, M.T., MANNION, P.D., SULLIVAN, C., UPCHURCH, P. & EVANS, D.C. 2014. Rates of dinosaur body mass evolution indicate 170 million years of sustained ecological innovation on the avian stem lineage. *PLOS Biology* **12**(5), e1001853.

BENSON, R.B., HUNT, G., CARRANO, M.T. & CAMPIONE, N. 2017. Cope's rule and the adaptive landscape of dinosaur body size evolution. *Palaeontology* **61**(1), 13–48.
BERCHTOLD, B.W. & PRESL, J. 1820. *O Přirozenofti Roftlin* [Jan-Apr] **1820**, 1–322, err.
BONAPARTE, J.F. 1971. Los tetrapodos del sector superior de la formacion Los Colorados, la Rioja, Argentina (Triásico Superior) I Parte. *Opera Lillona* **22**, 1–183.
BORDY, E.M., ABRAHAMS, M., SHARMAN, G.R., VIGLIETTI, P.A., BENSON, R.B., McPHEE, B.W., BARRETT, P.M., SCISCIO, L., CONDON, D. & MUNDIL, R. 2020. A chronostratigraphic framework for the upper Stormberg Group: implications for the Triassic-Jurassic boundary in southern Africa. *Earth-Science Reviews* **203**, 103120.
BORDY, E.M. & ERIKSSON, P. 2015. Lithostratigraphy of the Elliot Formation (Karoo Supergroup), South Africa. *South African Journal of Geology* **118**(3), 311–316.
BORDY, E.M., HANCOX, J.P. & RUBIDGE, B.S. 2004. Basin development during the deposition of the Elliot formation (Late Triassic-Early Jurassic), Karoo supergroup, South Africa. *South African Journal of Geology* **107**(3), 397–412.
BOTHA, J., CHOINIERE, J.N. & BENSON, R.B. 2022. Rapid growth preceded gigantism in sauropodomorph evolution. *Current Biology* **32**(20), 4501–4507.
BREMER, K. 1994. Branch support and tree stability. *Cladistics* **10**(3), 295–304.
BRONGNIART, A. 1828. *Prodrome d'une histoire des végétaux fossiles*. Paris, F.G. Levrault.
BRONGNIART, A. 1843. *Enumération des Genres de Plantes cultivés au Muséum d'Histoire Naturelle de Paris. Fortin*. Paris, Masson et Cie.
BRONGNIART, A. 1849. *Tableau des genres de végétaux fossiles considérés sous le point de vue de leur classification botanique et de leur distribution géologique*. Paris, Imprimerie de L. Martinet.
BUTLER, R.J., BARRETT, P.M., KENRICK, P. & PENN, M.G. 2009. Testing co-evolutionary hypotheses over geological timescales: interactions between Mesozoic non-avian dinosaurs and cycads. *Biological Reviews* **84**(1), 73–89.
CAMPIONE, N.E. & EVANS, D.C. 2012. A universal scaling relationship between body mass and proximal limb bone dimensions in quadrupedal terrestrial tetrapods. *BMC Biology* **10**(1), 60.
CAMPIONE, N.E., EVANS, D.C., BROWN, C.M. & CARRANO, M.T. 2014. Body mass estimation in non-avian bipeds using a theoretical conversion to quadruped stylopodial proportions. *Methods in Ecology and Evolution* **5**(9), 913–923.
CERDA, I.A., CHINSAMY, A., POL, D., APALDETTI, C., OTERO, A., POWELL, J.E. & MARTÍNEZ, R.N. 2017. Novel insight into the origin of the growth dynamics of sauropod dinosaurs. *PLOS ONE* **12**(6), e0179707.
DOI: 10.1371/journal.pone.0179707
CHAPELLE, K.E.J., BARRETT, P.M., BOTHA, J. & CHOINIERE, J.N. 2019. *Ngwevu intloko*: a new early sauropodomorph dinosaur from the Lower Jurassic Elliot Formation of South Africa and comments on cranial ontogeny in *Massospondylus carinatus*. *PeerJ* **7**, e7240.
DOI: 10.7717/peerj.7240
CHAPELLE, K.E.J., BENSON, R.B., STIEGLER, J., OTERO, A., ZHAO, Q. & CHOINIERE, J.N. 2020. A quantitative method for inferring locomotory shifts in amniotes during ontogeny, its application to dinosaurs and its bearing on the evolution of posture. *Palaeontology* **63**(2), 229–242.
CHAPELLE, K.E.J., BOTHA, J. & CHOINIERE, J.N. 2021. Extreme growth plasticity in the early branching sauropodomorph *Massospondylus carinatus*. *Biology Letters* **17**(5), 20200843.
CLEAL, C.J. & REES, P.M. 2003. The Middle Jurassic flora from Stonesfield, Oxfordshire, UK. *Palaeontology* **46**(4), 739–801.
DOWELD, A. 2001. *Prosyllabus Tracheophytorum: Tentamen Systematis Plantarum Vascularium Tracheophy.* Moscow, GEOS.
GALTON, P.M., HEERDEN, J.V. & YATES, A.M. 2005. Postcranial anatomy of referred specimens of the sauropodomorph dinosaur *Melanorosaurus* from the Upper Traissic of South Africa. **In**: Tidwell, V. & Carpenter K. (eds), *Thunder Lizards*, 1–37. Bloomington, Indiana University Press.
GOLOBOFF, P.A., CARPENTER, J.M., ARIAS, J.S. & ESQUIVEL, D.R.M. 2008. Weighting against homoplasy improves phylogenetic analysis of morphological data sets. *Cladistics* **24**(5), 758–773.
GOLOBOFF, P.A. & CATALANO, S.A. 2016. TNT version 1.5, including a full implementation of phylogenetic morphometrics. *Cladistics* **32**(3), 221–238.
GRIFFIN, C.T., WYND, B.M., MUNYIKWA, D., BRODERICK, T.J., ZONDO, M., TOLAN, S., LANGER, M.C., NESBITT, S.J. & TARUVINGA, H.R. 2022. Africa's oldest dinosaurs reveal early suppression of dinosaur distribution. *Nature* **609**(7926), 313–319.
HANCOX, P.J., NEVELING, J. & RUBIDGE, B.S. 2020. Biostratigraphy of the *Cynognathus* Assemblage Zone (Beaufort Group, Karoo Supergroup), South Africa. *South African Journal of Geology 2020* **123**(2), 217–238.
HARMON, L., WEIR, J., BROCK, C., GLOR, R., CHALLENGER, W., HUNT, G., FITZJOHN, R., PENNELL, M., SLATER, G. & BROWN, J. 2007. The geiger package: analysis of evolutionary diversification, v. 0.2-6.
http://cran.r-project.org/
HAUGHTON, S. 1924. The fauna and stratigraphy of the Stormberg Series. *Annals of the South African Museum* **12**(8), 323–497.
HUENE, F.V. 1932. Die fossile Reptil-Ordnung Saurischia, ihre Entwicklung und Geschichte. *Monographien zur Geologie und Paläontologie* **1**, 1–361.
KITCHING, J.W. & RAATH, M.A. 1984. Fossils from the Elliot and Clarens Formations (Karoo Sequence) of the northeastern Cape, Orange Free State and Lesotho, and a suggested biozonation based on tetrapods. *Palaeontologia africana* **25**, 111–125.
KVAČEK, J. & STRAKOVÁ, M. 1997. *Catalogue of Fossil Plants Described in Works of Kaspar M. Sternberg*. Prague, National Museum .
LABANDEIRA, C.C., ANDERSON, J.M. & ANDERSON, H.M. 2018. Expansion of arthropod herbivory in Late Triassic South Africa: the Molteno Biota, Aasvoëlberg 411 site and developmental biology of a gall. **In**: Tanner, L.H. (ed), *The Late Triassic World: Earth in a Time of Transition*, 623–719. Springer Link.
LABANDEIRA, C.C., WILF, P., JOHNSON, K.R. & MARSH, F. 2007. Guide to insect (and other) damage types on compressed plant fossils. Washington DC, National Museum of Natural History, Smithsonian Institution.
MADDISON, W. & MADDISON, D. 2019. Mesquite: a modular system for evolutionary analysis. Version 3.61.
https://mesquiteproject.org
McPHEE, B.W., BENSON, R.B., BOTHA-BRINK, J., BORDY, E.M. & CHOINIERE, J.N. 2018. A giant dinosaur from the earliest Jurassic of South Africa and the transition to quadrupedality in early sauropodomorphs. *Current Biology* **28**(19), 3143–3151. e7.
McPHEE, B.W., BONNAN, M.F., YATES, A.M., NEVELING, J. & CHOINIERE, J.N. 2015a. A new basal sauropod from the pre-Toarcian Jurassic of South Africa: evidence of niche-partitioning at the sauropodomorph–sauropod boundary? *Scientific Reports* **5**, 13224.
McPHEE, B.W., BORDY, E.M., SCISCIO, L. & CHOINIERE, J.N. 2017. The sauropodomorph biostratigraphy of the Elliot Formation of southern Africa: tracking the evolution of Sauropodomorpha across the Triassic–Jurassic boundary. *Acta Palaeontologica Polonica* **62**(3), 441–465.
McPHEE, B.W., CHOINIERE, J.N., YATES, A.M. & VIGLIETTI, P.A. 2015b. A second species of *Eucnemesaurus* Van Hoepen, 1920 (Dinosauria, Sauropodomorpha): new information on the diversity and evolution of the sauropodomorph fauna of South Africa's lower Elliot Formation (latest Triassic). *Journal of Vertebrate Paleontology* **35**(5), e980504.
McPHEE, B.W., YATES, A.M., CHOINIERE, J.N. & ABDALA, F. 2014. The complete anatomy and phylogenetic relationships of *Antetonitrus ingenipes* (Sauropodiformes, Dinosauria): implications for the origins of Sauropoda. *Zoological Journal of the Linnean Society* **171**(1), 151–205.
MOSER, M. 2003. *Plateosaurus engelhardti* Meyer, 1837 (Dinosauria: Sauropodomorpha) aus dem Feuerletten (Mittelkeuper; Obertias) von Bayern. *Zitteliana, Reihe B* **24**, 1–186.
OLSEN, P.E. & GALTON, P.M. 1984. A review of the reptile and amphibian assemblages from the Stormberg of southern Africa, with special emphasis on the footprints and the age of the Stormberg. *Palaeontologia africana* **25**, 87–110.
OTERO, A. & HUTCHINSON, J.R. 2022. Body size evolution and locomotion in Sauropodomorpha: what the South American record tells us. **In**: *South American Sauropodomorph Dinosaurs*, 443–472. Springer.
OTERO, A. & POL, D. 2013. Postcranial anatomy and phylogenetic relationships of *Mussaurus patagonicus* (Dinosauria, Sauropodomorpha). *Journal of Vertebrate Paleontology* **33**(5), 1138–1168.
OWEN, R. 1842. Report on British fossil reptiles. *Report of the British Association of Advanced Sciences* **9**, 60–204.
PEYRE DE FABRÈGUES, C. & ALLAIN, R. 2016. New material and revision of *Melanorosaurus thabanensis*, a basal sauropodomorph from the Upper Triassic of Lesotho. *PeerJ* **4**, e1639.
PEYRE DE FABRÈGUES, C. & ALLAIN, R. 2020. *Kholumolumo ellenbergerorum*, gen. et sp. nov., a new early sauropodomorph from the lower Elliot Formation (Upper Triassic) of Maphutseng, Lesotho. *Journal of Vertebrate Paleontology* **39**(6), e1732996.
DOI: 10.1080/02724634.2019.1732996
PLUMSTEAD, E.P. 1969. Three thousand million years of plant life in

Africa. Alex L. du Toit Memorial Lectures No. 1. *Transactions of the Geological Society of South Africa*, *Annexure to* **72**.
POL, D., MANCUSO, A.C., SMITH, R.M.H., MARSICANO, C.A., RAMEZANI, J., CERDA, I.A., OTERO, A. & FERNANDEZ, V. 2021a. Earliest evidence of herd-living and age segregation amongst dinosaurs. *Scientific Reports* **11**(1), 20023.
DOI: 10.1038/s41598-021-99176-1
POL, D., OTERO, A., APALDETTI, C. & MARTÍNEZ, R.N. 2021b. Triassic sauropodomorph dinosaurs from South America: the origin and diversification of dinosaur dominated herbivorous faunas. *Journal of South American Earth Sciences* **107**, 103145.
POL, D. & POWELL, J.E. 2007. New information on *Lessemsaurus sauropoides* (Dinosauria: Sauropodomorpha) from the Upper Triassic of Argentina. *Special Papers in Palaeontology* **77**, 223.
SANDER, P.M., GEE, C.T., HUMMEL, J. & CLAUSS, M. 2010. Mesozoic plants and dinosaur herbivory. *Plants in Mesozoic Time: Morphological Innovations*, *Phylogeny*, *Ecosystems*, 331–359.
SCISCIO, L., BRODERICK, T.J., BARRETT, P.M., MUNYIKWA, D., ZONDO, M. & CHOINIERE, J.N. 2021. Invertebrate and plant trace fossils from the terrestrial Late Triassic of Zimbabwe. *PALAIOS* **36**(4), 129–140.
SCOTT, A.C., ANDERSON, J.M. & ANDERSON, H.M. 2004. Evidence of plant–insect interactions in the Upper Triassic Molteno Formation of South Africa. *Journal of the Geological Society* **161**(3), 401–410.
SEELEY, H.G. 1888. The classification of the Dinosauria. *Report of the British Association for the Advancement of Science* **57**, 698–699.
VAN KONIJNENBURG-VAN CITTERT, J.H.A., POTT, C., CLEAL, C.J. & ZIJLSTRA, G. 2017. Differentiation of the fossil leaves assigned to *Taeniopteris*, *Nilssoniopteris* and *Nilssonia* with a comparison to similar genera. *Review of Palaeobotany and Palynology* **237**, 100–106.
VIGLIETTI, P., McPHEE, B., BORDY, E., SCISCIO, L., BARRETT, P., BENSON, R., WILLS, S., CHAPELLE, K., DOLLMAN, K. & MDEKAZI, C. 2020a. Biostratigraphy of the *Massospondylus* Assemblage Zone (Stormberg Group, Karoo Supergroup), South Africa. *South African Journal of Geology 2020* **123**(2), 249–262.
VIGLIETTI, P., McPHEE, B., BORDY, E., SCISCIO, L., BARRETT, P., BENSON, R., WILLS, S., TOLCHARD, F. & CHOINIERE, J. 2020b. Biostratigraphy of the *Scalenodontoides* Assemblage Zone (Stormberg Group, Karoo Supergroup), South Africa. *South African Journal of Geology* **123**(2), 239–248.
WILSON, J.A. 1999. A nomenclature for vertebral laminae in sauropods and other saurischian dinosaurs. *Journal of Vertebrate Paleontology* **19**(4), 639–653.
WILSON, J.A., MICHAEL, D., IKEJIRI, T., MOACDIEH, E.M. & WHITLOCK, J.A. 2011. A nomenclature for vertebral fossae in sauropods and other saurischian dinosaurs. *PLOS ONE* **6**(2), e17114.
YATES, A.M., WEDEL, M.J. & BONNAN, M.F. 2012. The early evolution of postcranial skeletal pneumaticity in sauropodomorph dinosaurs. *Acta Palaeontologica Polonica* **57**(1), 85–100.
DOI: 10.4202/app.2010.0075
YOUNG, C-C. 1942. *Yunnanosaurus huangi* Young (gen. et sp. nov.), a new Prosauropoda from the Red Beds at Lufeng, Yunnan. *Bulletin of the Geological Society of China* **22**(122), 63–104.